PRESSURE RATIO IMPACT AND INTERMEDIATE PERSSURE OF COMPRESSIBLE FLUID FLOW THROUGH MULTIPLE SINGLE ORIFICE RESTRICTORS IN SERIES

(NUMERICAL ANALYSIS)

Ian Navin

Engineering Project
Submitted in Partial Fulfillment of the Requirements for the Degree of

Master of Engineering in Mechanical Engineering

Approved by:
Dr. Francisco Cunha, PhD, PE

Department of Mechanical, Aerospace, and Nuclear Engineering
Rensselaer Polytechnic Institute
Troy, New York

[December 2022]

Submitted November 2022

TABLE OF CONTENTS

LIST OF SYMBOLS

a	Acoustic Speed or Speed of Sound
a_o	Speed of Sound - Stagnation
a^*	Speed of Sound - Critical
a	Acceleration
A	Area
B	Body Force
C_d	Coefficient of Discharge
c_p	Specific Heat at Constant Pressure
c_v	Specific Heat at Constant Volume
D	Drag Force
e	Specific Stored Energy
E	Stored Energy
F	Force
F_c	Compressibility Factor
g	Gravity
G	Mass Flux
γ	Specific Heat Ratio
h	Specific Enthalpy
i, j, k	Unit vectors in x, y, and z directions
I	Volumetric Flow (SCFM)
m	Mass
$\dot{m}$	Mass Flow Rate
M	Mach Number
M	Momentum
p	Pressure
P	Stagnation pressure
p^*	Critical Pressure
ρ	Density
ρ_o	Stagnation Density
ρ^*	Critical Density
Q	Heat
R	Gas Constant
s	Specific Entropy
S	Entropy
t	Temperature
T	Stagnation Temperature
t^*	Critical Temperature
u	Specific Internal Energy or Velocity in x
U	Internal Energy
$\mathcal{V}$	Specific Volume
v	Velocity in y
V	Volume
V	Velocity

w	Velocity in z
W	Work
Ω	Flow Resistance

LIST OF TABLES

LIST OF FIGURES

ABSTRACT

In the previous report, the study of compressible flow through a single orifice was conducted starting with the theory and background of fluid and gas dynamics. After applying the known discharge coefficients and target orifice size (Ø 0.0007”) to the derived sonic and subsonic flow rate equations, an equivalent size orifice (Ø 0.0007”) was produced using a laser. A pressure ratio vs flow rate curve was drawn for the laser drilled hole and compared to the theoretical flow of a sharp edge and a round edge hole. There was some disagreement between the two coefficients of discharge, but this may be due to the many assumptions made of the fluid such as the fluid was adiabatic, frictionless, reversible, and perfect. Conducting a numerical analysis of compressible fluid through multiple orifices in series was studied as an extension of the single orifice using Siemens FloEFD Software. CFD models were validated using the single orifice restrictor model and comparing to the theoretical and experimental values found in the first report. With mesh optimization and careful selection of boundary conditions, the curve was validated to match the experimental values, though some of the pressure ratios were shifted slightly. With the validation of the single orifice, a multiple orifice model was constructed and optimized. Through parametric studies, the impact on the pressure ratios was evaluated to see when and where the flow was sonic and subsonic depending on the ratio of the orifice sizes. Of high interest with multiple orifices in series is the intermediate pressure between the restrictors. Previous work was conducted by The Lee Company [6], and through CFD analysis, the work was confirmed with close agreement to 1.6% with a maximum of 6% error. Future work using computational fluid dynamics can build upon two orifices in series to use infinitely more orifices and also explore gases of differing densities, as well as increased orifice sizing.

1.0 INTRODUCTION

1.1 Project Background

Precision fluid flow has recently expanded to pneumatic systems for the space industry. These space applications require precision fluid metering for systems such as ion propulsion. With the limited capacity to store fuel such as Krypton and Xenon, efficiency is critical. These systems utilize precision fluid flow elements like sharp edge orifice restrictors to meter flow. As explored in the prior report [1], efficiency of these systems can be measured by the conditions at the orifice characterizing as sonic or subsonic flow. To aid in this characterization, an understanding of the pressure upstream and downstream each orifice, including the intermediate pressure in between the orifices. The study of the pressure ratio impact of a single orifice restrictor is valuable to understand the basics of compressible fluid flow in such passages, but to capture the greater picture, a higher restriction with a larger orifice should be explored.

As previously discussed in the compressible fluid flow through a single orifice restrictor, propulsion systems such as Ion thrusters (see Figure 1) use inert gases and electrical power to produce ionization of electrons and propellant atoms which create positively charged ions that propel through charged grids, which forces the craft forward. Any positively charged ions that pass through the grid are then neutralized by electrons. Though the thrust produced is very low, over time the craft can reach high velocities, “90,000 meters per second (over 200,000 mph)” [13] which is ideal for environments such as space. The electrons and propellant atoms are discharged from the propellant management system which consists of precision metering elements called the anode and cathode (or neutralizer). Efficiency of these orifices is key as the craft only has a finite amount of fuel on board. Understanding the flow conditions, as well as the ratios of fuel to utilize are

essential for efficiency. The best way to predict that precision flow is through a highly restrictive component that will operate in the sonic region for as long as possible, which will result in a more consistent flow in and out of the discharge chamber. Most times, the high restriction is achieved with multiple orifices since these orifices in series can produce the same restriction as a single orifice, but with larger passage sizes, which can be ideal when considering contamination like foreign object debris. Protecting small single orifices can also be a manufacturing challenge as producing this orifice and protecting it during manufacturing and while performing in a customer system with some sort of screen can prove to be difficult. Understanding the theory behind the compressible fluid flow in both the sonic and subsonic state through a highly restrictive orifice plate leads the way to discovering the impacts of multiple orifices in series. As even a single orifice plate proved difficult to produce for experimental purposes and very technical for a theoretical methodology of compressible fluid flow as the intermediate pressures between orifices needs to be found since the compressibility of the fluid causes an uneven pressure drop over the orifices, a numerical approach will be utilized to study multiple orifices.

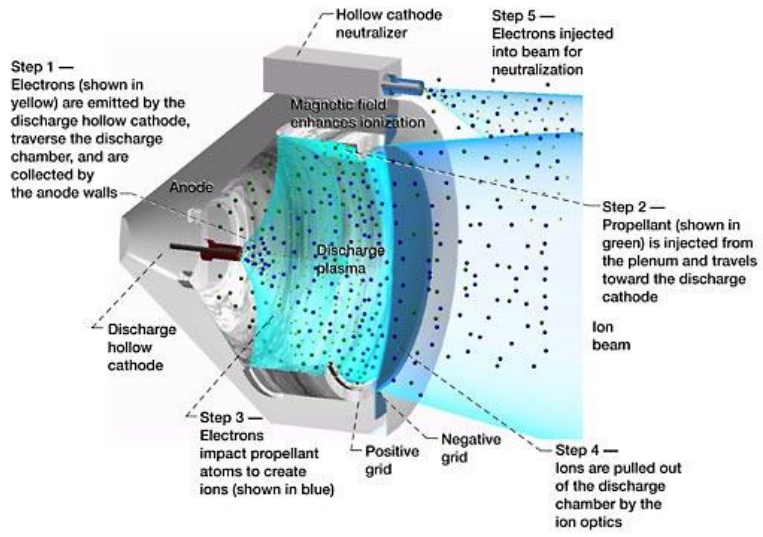

Figure 1: Ion Thruster Operation Steps [14]

1.2 Assumptions

To accurately solve this problem using computation fluid dynamics (CFD), I will use Siemens FloEFD software which is compatible with SolidWorks where modeling of the system can be conducted. We also must methodically progress through the model difficulty to ensure that our model, environment, initial conditions, boundary conditions, and goals are set up correctly. To start, the information obtained from the previous study of compressible fluid flow theoretically and experimentally on a single orifice [1] will be modeled, analyzed in CFD, and compared. Once validated, the analysis can move to evaluating two orifices in series and the impact of the restriction ratio of the two orifices on the intermediate pressure.

Before modeling and using the CFD software, we must consider some assumptions; most taken from the initial report [1], but some new for the expanded analysis. We will be looking at a steady one-dimensional inviscid compressible fluid flow with a constant sharp orifice geometry (with a coefficient of discharge of 0.65 as found empirically) including the minimum diameter of 0.0007". The thickness of the plate will be a minimum of 0.0055". We will also consider an isentropic flow which assumes an adiabatic and reversible flow and expansion through the orifice. In this type of flow, the work transfer of the system is frictionless, and no net transfer of heat or matter will occur. The fluid and surrounding bodies are in thermal equilibrium. We also assume that no condensation at the orifice occurs or any effects of radiation. To perform the analysis through a numerical approach correctly, we will assume a constant uniform inlet mass flow rate equal to the mass flow rate found empirically. We assume that the lowest downstream pressure is just above atmosphere at 15.3 psia (P2). The largest upstream pressure to be considered for the single orifice analysis initially will be 100 psia (P1) (yielding a max pressure ratio ($\frac{P_1}{P_2}$) of 6.8). The numerical analysis

will first consider nitrogen gas and potentially other noble gases, though nitrogen gas was used for the experimental portion of the analysis. To solve for mass flow from the volumetric flow found experimentally, we will need the density of the fluid, which we will assume to be 0.074 $\frac{lb_m}{ft^3}$.

During the setup, we will utilize the downstream pressures and flow rates (converted to mass flow) measured during the experimental testing in our boundary conditions. After validating the 0.0007" orifice plate, a larger hole sizes will be considered yielding restriction ratios of 0.5, 1, 2, 4, and 10 which is more representative of orifice combinations used in multi-orifice restrictors for similar gas systems.

1.3 Previous Work

Upon research, previous work was scarce, though some work had been published by The Lee Company to aid in customer selection of restrictors in series [6]. The work focused on the intermediate pressure when two restrictors are in series. It estimates this based on the ratio of the restrictions based on theoretical calculations. This work was specifically targeted as an initial understanding of the intermediate pressure of orifices in series. If the work could be reproduced using numerical analysis, then this study could be expanded to look at the impact of more orifices in series (three, four, five, etc). This would lend itself well to customers of the space industry who utilize high restriction orifices in this fashion in their systems.

Previous work relating to the pressure ratio impact on orifices in series was not found. The study in this report does explore this after validating the single orifice pressure ratio impacts using the numerical analysis in the computational fluid dynamic software.

2.0 CONCLUSIONS

The purpose of this report is to analyze the flow of a compressible fluid through multiple sharp edge orifices that are arranged in series using a numerical approach. With an understanding of a numerical approach and of the multiple restrictors in series, customers system efficiency and performance is more easily predictable. The use of the numerical study allows the future expansion of orifices in series and also in parallel configurations without deriving complex equations or manufacturing and testing these precise orifices.

In order to perform the numerical analysis on multiple orifices, the work conducted in the previous report must be validated using the CFD software. The previous report work, theoretically and experimentally, was reviewed and summarized which allowed the start of the numerical analysis. The setup in the computational fluid dynamics software is crucial to the program working correctly. The mass flow rate was set at the inlet of the model and the known downstream pressure was also set which allowed the upstream pressure to be solved for. Prior to starting the evaluation of multiple downstream pressures and mass flow rates, a convergence study was conducted. This convergence study ensured that the mesh was optimally set to produce the correct result.

After the mesh convergence study, a parametric study was conducted for all of the mass flows and downstream pressures in the experimental testing. This created eight design points where the results matched the theoretical flow curve with the upstream pressures as shown in Figure 2.

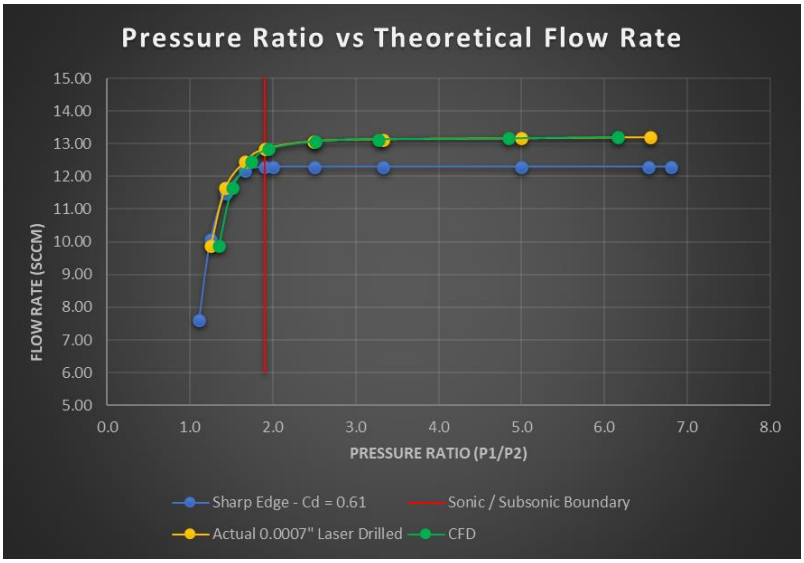

Figure 2: Single Orifice CFD Curve vs Theoretical and Experimental

With the single orifice validated, the CFD software was used to model and analyze two orifices in series to see the pressure ratio impact as well as the intermediate pressures of orifice ratios of 0.5, 1, 2, 4, and 10. The setup was similar to the single orifice except another surface goal for total pressure was added. The results for the pressure ratio impact can be seen in Table 17 and the intermediate pressures plot can be seen in Figure 3 below.

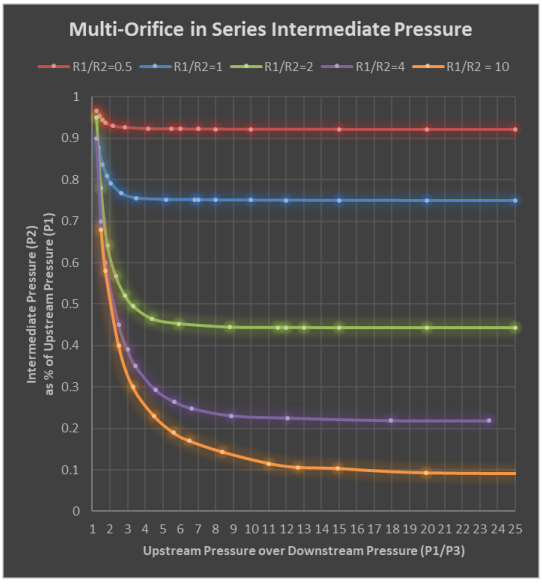

Figure 3: Overall Pressure Ratio (P1/P3) vs Intermediate Pressure as % of P1

Customers that will be designing in orifices in series can now use this plot to determine the intermediate pressures and the flow characteristic of sonic or subsonic at different orifice locations and ratios. Future work will focus on the integration of more orifices in series and orifices situated in parallel.

3.0 ANALYSIS

To be able to solve a gas dynamics problem, we must first understand the fundamentals of fluid dynamics. The equations and derivations performed in the previous analysis of a single orifice restrictor [1] were closely followed by the Gas Dynamics text by Maurice Zucrow [2], though these derivations have been completed in many other texts and sources. The background and fundamentals can be summarized in the following sections for clarity.

3.1 Fundamentals and Background

Derivations started from the conservation of mass, momentum, and energy as well as the second law of thermodynamics which aids in defining entropy. Using our boundary conditions, we can further simplify these equations before deriving the integral forms which are useful “as they can be applied to any type of fluid flow situation” [1].

A summary of the derived equations can be found in Table 1. For any specifics pertaining to the derivation of these equations and application of assumptions and boundary conditions can be found in the previous supporting report [1].

Equation Name	**Equation Form**	**Equation Number**
Conservation of Mass (Integral Form)	$\int_{\mathcal{V}} \frac{d\rho}{dt} d\,\mathcal{V} + \int_A \rho d\mathcal{V} \cdot dA = 0$	(1)
Steady Flow Conservation of Mass (Integral Form)	$\int_A \rho d\mathcal{V} \cdot dA = 0$	(2)
Conservation of Momentum (Integral Form)	$\int_{\mathcal{V}} \boldsymbol{B}\rho\, dV - \int_A p\, d\boldsymbol{A} + \boldsymbol{F}_{shear} = \int_{\mathcal{V}} (\rho \boldsymbol{V})_t dV + \int_A \boldsymbol{V}(\rho \boldsymbol{V} \cdot d\boldsymbol{A})$	(3)
Steady Flow Conservation of Momentum (Integral Form)	$\int_{\mathcal{V}} (\rho u_i)_t dV = 0$	(4)
Conservation of Energy (Integral Form)	$\dot{W}_{shaft} + \dot{W}_{shear} - \dot{Q} + \int_{\mathcal{V}} \frac{\partial}{\partial t} [\rho \left(u + \left(\frac{V^2}{2} \right) + gz \right) d\mathcal{V} + \int_A [\rho \left(h + \left(\frac{V^2}{2} \right) + gz \right) (\rho \boldsymbol{V} \cdot d\boldsymbol{A}) = 0$	(5)
Entropy Equation (Integral Form)	$\int_{\mathcal{V}} (s\rho)_t d\mathcal{V} + \int_A s(\rho \boldsymbol{V} \cdot d\boldsymbol{A}) = \frac{\dot{Q}}{t}$	(6)

Table 1: Derived Integral Form Equations [1]

3.2 One-Dimensional Steady Flow

Further simplifying the equations in Table 1 can be applied by introducing assumptions to the integral forms which include one-dimensional steady flow and the neglect of body forces. We also will be evaluating these equations through a stream tube as shown in Figure 2, a differential element of the stream tube as shown in Figure 3, and differential fluid element as shown in Figure 4. This transforms the equations to forms more manageable.

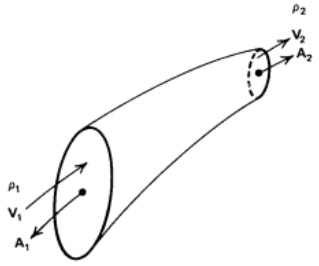

Figure 4: Generic Stream Tube [2]

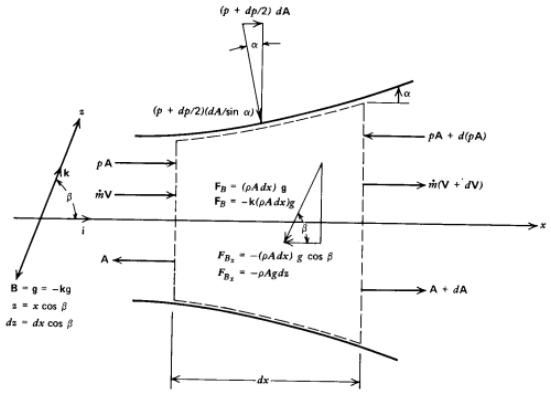

Figure 5: Differential Element of Stream Tube (1D Fluid Flow) [2]

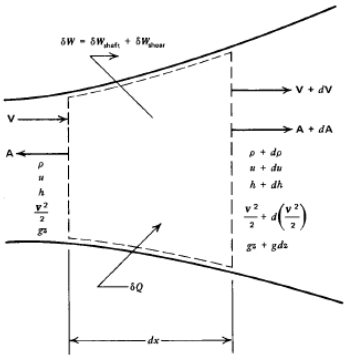

Figure 6: Energy Balance of Differential Fluid Element [2]

Equation Name	**Equation**	**Equation Number**
Mass Flow Through Stream Tube (1D)	$\dot{m} = \rho_1 A_1 V_1 = \rho_2 A_2 V_2 = \rho A V = constant$	(7)
Bernoulli Equation (1D Steady Inviscid Fluid)	$dp + \rho V dV + \rho g dz = 0$	(8)
Bernoulli Constant (1D Steady Inviscid Fluid)	$\int \frac{dp}{\rho} + \frac{V^2}{2} + gz = constant$	(9)
Bernoulli Equation (Incompressible Fluid)	$\frac{p}{\rho} + \frac{V^2}{2} + gz = constant$	(10)
Energy Equation (1D Steady, Isentropic Flow)	$\frac{dp}{\rho} + d\left(\frac{V^2}{2}\right) + gdz = 0$	(11)

Table 2: Equation Transformations with Applied Assumptions [1]

Equations 8 and 9 "can be applied to both compressible and incompressible flows, which yields differing results depending on the Mach number. The Mach number is defined as the local velocity divided by the speed of sound of the fluid" [1].

$$M = \frac{V}{a} \quad \textbf{(12)}$$

As explained in the previous report "When the local velocity ratio to the speed of sound is less than one, it is subsonic, equal to one is sonic, and greater than one is known as supersonic. Using the Mach number in calculations is advantageous since if it is known, then many of the critical parameters such as the critical pressure, density, and temperature can be calculated." [1].

When discussing sonic and supersonic flow conditions of a compressible fluid, it is useful to show the flow properties using the Mach number relationship as seen in Table 3 which reflect an adiabatic inviscid fluid (also known as isentropic).

Equation Name	Equation	Equation Number
Bernoulli's Equation (Isentropic Flow)	$\frac{d\rho}{\rho} + M^2\left(\frac{dV}{V}\right) = 0$	(13)
Energy Equation (Isentropic Flow)	$dh + d\left(\frac{V^2}{2}\right) + gdz = 0$	(14)
Energy Equation (Perfect Gas)	$c_p t + \left(\frac{V^2}{2}\right) = constant$	(15)

Table 3: Isentropic Flow and Mach Number Applied [1]

Applying the Mach number, $M = \frac{V}{a}$, into the equations 15, we use a few relationships. These include R, the universal gas constant, the specific heat ratio, $\gamma = \frac{c_p}{c_v}$, where the constant pressure of a perfect gas is $c_p = \frac{\gamma R}{\gamma - 1}$ and $a^2 = \gamma R t$ yielding differing forms of the energy equation for the adiabatic flow of a perfect gas as shown in Table 4.

Equation Name	Equation	Equation Number
Energy Equation (Form 1)	$\frac{V^2}{2} + \frac{a^2}{\gamma - 1} = constant$	(16)
Energy Equation (Form 2)	$a^2\left(1 + \frac{\gamma - 1}{2}M^2\right) = constant$	(17)
Energy Equation (Form 3)	$t\left(1 + \frac{\gamma - 1}{2}M^2\right) = constant$	(18)

Table 4: Forms of the Energy Equation - Adiabatic Flow of Perfect Gas [1]

3.3 Compressible Fluid Flow Critical Conditions

When discussing compressible fluid flow, it is important to discuss the stagnation conditions. As discussed in the first report on compressible flow through a single orifice, "there can come a point where the velocity reaches zero. For differing parameters where the speed of the gas is adiabatically decelerated to zero, we call these the stagnation points or conditions. This is called stagnation because the fluid will be stagnant in this state as it will not be moving. The stagnation conditions that can be in the form of temperature, pressure, enthalpy, density, and acoustic speed" [1]. These equations are summarized below in Table 5.

Equation Name	**Equation**	**Equation Number**
Stagnation Temperature	$T = t\left(1 + \frac{\gamma - 1}{2} M^2\right)$	(19)
Stagnation Pressure	$\frac{P}{p} = \left(\frac{T}{t}\right)^{\frac{\gamma}{\gamma-1}} = \left(1 + \frac{\gamma - 1}{2} M^2\right)^{\frac{\gamma}{\gamma-1}}$	(20)
Stagnation Density	$\frac{\rho_o}{\rho} = \left(1 + \frac{\gamma - 1}{2} M^2\right)^{\frac{1}{\gamma-1}}$	(21)
Stagnation Enthalpy	$H = (h_2)_{V_2=0} = h + \frac{V^2}{2}$	(22)

Table 5: Stagnation Condition Equations for Isentropic Perfect Gas [1]

Furthermore, these stagnation conditions allowed us to determine the critical conditions where the fluid that is originally subsonic reaches sonic conditions at $M = 1$. The critical mass flow condition, where the maximum mass flow is achieved when the critical speed of sound is reached, is also derived where we use the continuity of mass equation in conjunction with the stagnation pressure and the critical area ratio (local area over critical area) as shown in equation 23.

$$\frac{A}{A^*} = \frac{1}{M}\left[\frac{2}{\gamma+1}\left(1+\frac{\gamma-1}{2}M^2\right)\right]^{\frac{\gamma+1}{2(\gamma-1)}} \tag{23}$$

All critical conditions are shown using an Asterix and are all shown in Table 6.

Equation Name	**Equation**	**Equation Number**
Critical Temperature	$t^* = \frac{2}{\gamma+1}T$	(24)
Critical Pressure	$p^* = P\left(\frac{t^*}{T}\right)^{\frac{\gamma}{\gamma-1}} = P\left(\frac{2}{\gamma+1}\right)^{\frac{\gamma}{\gamma-1}}$	(25)
Critical Density	$\rho^* = \rho\left(\frac{p^*}{P}\right)^{\left(\frac{1}{\gamma}\right)} = \rho\left(\frac{2}{\gamma+1}\right)^{\frac{1}{\gamma-1}}$	(26)
Critical Mass Flow	$\dot{m}^* = \frac{PA^*}{\sqrt{\frac{\gamma}{RT}}}\gamma\left(\frac{2}{\gamma+1}\right)^{-\frac{\gamma+1}{2(\gamma-1)}}$	(27)

Table 6: Critical Conditions [1]

3.4 Compressible Flow in the Presence of an Area Change

To review the discussion of compressible flow in the presence of an area change from the previous report [1], we will show the area change of the single orifice in Figure 5. Of interest is the mass flow rate and the impacts of the downstream pressure at the subsonic, sonic, and supersonic conditions. As stated in the report on the single orifice restrictor [1], “It has been shown that when the mass flow enters the throat, and the backpressure can have an impact when in the subsonic flow conditions. This is due to disturbances in the pressure that is felt, and the fluid creates a jet stream. When the fluid reaches sonic speed conditions, the critical mass flow rate is achieved and become independent of the downstream pressure. This is referred to as the Rule of Forbidden Signals [5], which states, that the effect of pressure changes produced by a body moving at a speed faster than the speed of sound cannot reach points ahead of the body (von Kármán, Jour. Aero. Sci., Vol. 14, No. 7 (1947)). The body in our case is static, but the flow velocity reaches the speed of sound. With a downstream pressure that forces the flow to become sonic or reach a Mach number of unity, a change in the backpressure can’t reach points upstream of the throat” [1].

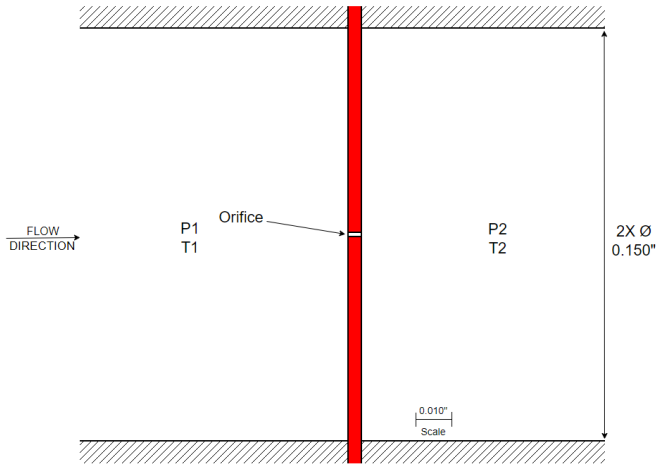

Figure 7: Orifice Plate Cross Section View of Area Change [1]

3.5 Flow Through and Orifice Plate and Resulting Restriction

Though Zucrow [1] provided the basics and the derivations of the critical conditions, Mark's Standard Handbook for Mechanical Engineers [3] was also considered, which states a similar derivation of the mass flow in the subsonic and sonic region. It was desired in the last report to represent the orifice by the restriction so the equation could be as simple as possible to handle. Mark's Standard Handbook [3] assumes that we have a single orifice with region 1 upstream the orifice, region 2 at the orifice, and region 3 downstream the orifice. Assuming an adiabatic reversible flow of a perfect gas, the mass flow in the subsonic region can be solved for as shown in Table 7. With the knowledge that the pressure ratio of 1.9 forces a sonic flow condition, the mass flow rate for the sonic condition is derived as shown in Table 7.

Equation Name	**Equation**	**Equation Number**
Subsonic Mass Flow Through an Orifice [3]	$m = C_d A_2 P_2 \frac{\left(\sqrt{\frac{2g}{RT}\left(\frac{\gamma}{\gamma-1}\right)\left(\frac{P_1}{P_2}\right)^{\frac{\gamma-1}{\gamma}}\left[\left(\frac{P_1}{P_2}\right)^{\frac{\gamma-1}{\gamma}}-1\right]}\right)}{\sqrt{1-\left(\frac{A_2}{A_1}\right)^2\left(\frac{P_2}{P_1}\right)^{\frac{2}{\gamma}}}}$	(28)
Sonic Mass Flow Through an Orifice [3]	$m = C_d A_2 P_1 \sqrt{\frac{g}{RT}\gamma\left(\frac{2}{\gamma+1}\right)^{\frac{\gamma+1}{\gamma-1}}}$	(29)

Table 7: Mass Flow Equations - Flow Through an Orifice Plate [1], [3]

The equations listed in Table 7 contain the C_d (discharge coefficient). From Mark's Standard Handbook for Engineers, a table shows the assumed values of the discharge coefficient of a few different edge conditions as shown in Figure 6.

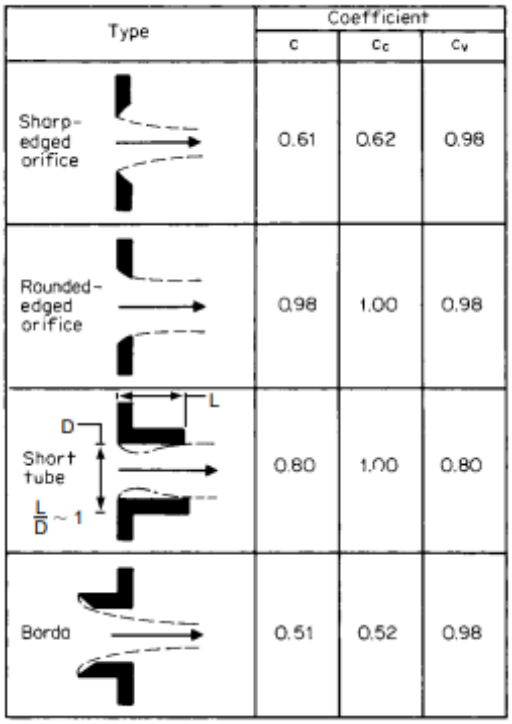

Figure 8: Coefficient of Discharge of Orifice Edge Conditions [1,3]

In the first report [1], the interest was of a sharp edge orifice, but since the rounded edge and sharp edge were so similar, both were used for theoretical calculations. Realistically since the disc thickness compared to the hole size is so great, the L/d ratio could have an impact, but the "short tube is not used since it assumes an L/d ratio of approximately 1.

To aid in simplifying the mass flow equation into volumetric flow and a unitless resistance, known relationships for resistance in incompressible fluid flow were used to find the resistance, Ω, and volumetric flow rate, *I*, for both subsonic and sonic conditions. These are shown in Table 8.

Equation Name	**Equation**	**Equation Number**
Resistance to Fluid Flow (Incompressible Fluids)	$$\Omega = \frac{20}{I}\sqrt{\frac{(P_1 - P_2)}{S}}$$	(30)
Resistance to Fluid Flow (Sonic)	$$\Omega = 43.927\left[\frac{P_1}{I\sqrt{T_1}}\right]\left[\gamma R\left(\frac{2}{\gamma+1}\right)^{\frac{\gamma+1}{\gamma-1}}\right]^{\frac{1}{2}}$$	(31)
Volumetric Flow (Sonic)	$$I = \frac{CP_1T_f}{\Omega} = \frac{CP_1T_f}{\frac{.5268}{C_dA}} = \frac{C_dACP_1T_f}{0.5268}$$ Where: $$B = 43.927\left[\gamma R\left(\frac{2}{\gamma+1}\right)^{\frac{\gamma+1}{\gamma-1}}\right]^{\frac{1}{2}}$$ $$C = \frac{B}{\sqrt{T_s}}$$ $$T_f = \sqrt{\frac{530}{T(°F)+460}}$$	(32)
Resistance to Fluid Flow (Subsonic)	$$\Omega = 62.16\frac{P_1}{\sqrt{T_1}I}\left[\left(\frac{\gamma R}{(\gamma-1)}\right)\left[\left(\frac{P_2}{P_1}\right)^{\frac{2}{\gamma}} - \left(\frac{P_2}{P_1}\right)^{\left(\frac{\gamma+1}{\gamma}\right)}\right]\right]^{\frac{1}{2}}$$	(33)
Volumetric Flow (Subsonic)	$$\mathrm{I} = \frac{CFP_1C_dA}{0.5268}$$ Where: $$F = 1.415\sqrt{\frac{\left[\left(\frac{P_2}{P_1}\right)^{\frac{2}{\gamma}} - \left(\frac{P_2}{P_1}\right)^{\left(\frac{\gamma+1}{\gamma}\right)}\right]}{(\gamma-1)\left(\frac{2}{\gamma+1}\right)^{\frac{\gamma+1}{\gamma-1}}}}$$	(34)

Table 8: Volumetric Flow and Resistance to Fluid Flow [1, 6]

Using the coefficient of discharge values and the volumetric flow equations from Table 8, the flows were calculated as shown in Table 9 and 10. It is assumed that the orifice is 0.0007 inches in diameter, $C = 276000$, $P_1 = 100\ psia$, $\gamma = 1.4\ for\ N_2$, $T = 70°F$.

P1	P2	Pressure Ratio	Flow Condition	Volumetric Flow (SCCM)
100	14.7	6.80	Sonic	12.30
	20	5.00	Sonic	12.30
	30	3.33	Sonic	12.30
	40	2.50	Sonic	12.30
	52.65	1.90	Sonic	12.30
	60	1.67	Subsonic	12.17
	70	1.23	Subsonic	11.47
	80	1.25	Subsonic	10.08
	90	1.11	Subsonic	7.60

Table 9: Theoretical Flow Rate of Single Orifice with Sharp Edge

P1	P2	Pressure Ratio	Flow Condition	Volumetric Flow (SCCM)
100	14.7	6.80	Sonic	19.76
	20	5.00	Sonic	19.76
	30	3.33	Sonic	19.76
	40	2.50	Sonic	19.76
	52.65	1.90	Sonic	19.76
	60	1.67	Subsonic	19.55
	70	1.23	Subsonic	18.43
	80	1.25	Subsonic	16.19
	90	1.11	Subsonic	12.20

Table 10: Theoretical Flow Rate of Single Orifice with Rounded Edge

Table 9 and 10 can be compared in a plot as shown in Figure 7. The boundary for the sonic to subsonic regions is split by the red vertical line, where the right side is the sonic region, and the left side is the subsonic region.

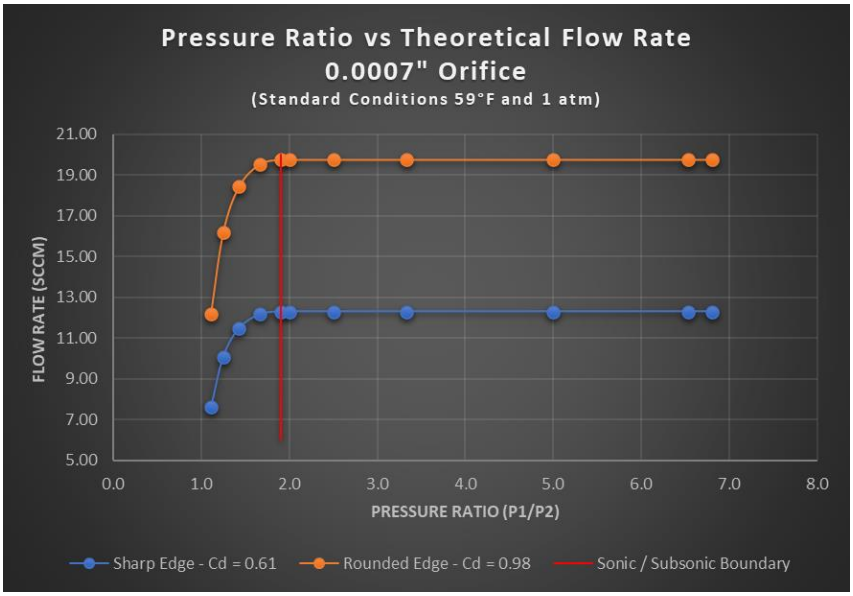

Figure 9: Pressure Ratio vs Theoretical Flow Rate (0.0007" Orifice)

3.6 Pressure Ratio vs Experimental Flow Rate of the Laser Drilled Orifice

To compare the theoretical calculations to an actual orifice, a laser was used. Figure 8 Shows the drilled hole at 2500X magnification.

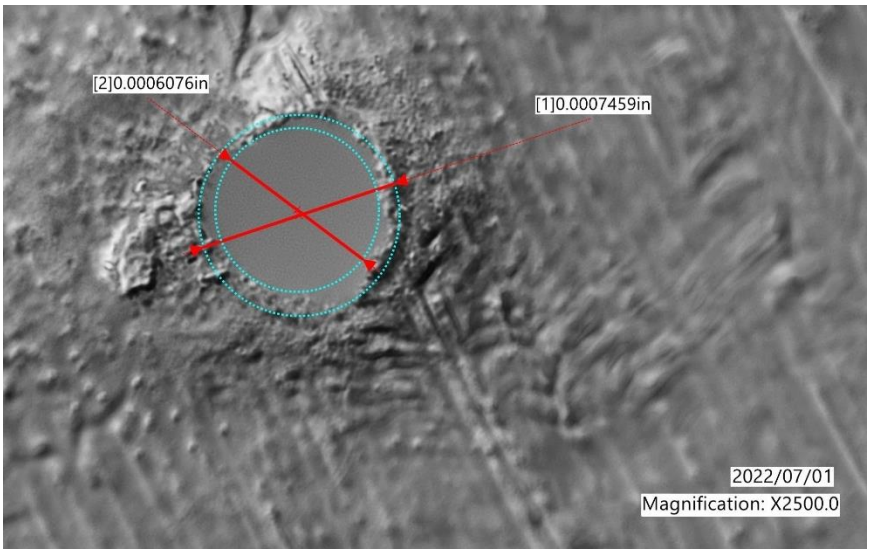

Figure 10: Laser Drilled Hole: Surface Texture with Min / Max Diameter

Next, the orifice was flowed with a backpressure regulator to do a downstream pressure sweep. The flow schematic can be seen in Figure 9, the flow results are found in Table 11, and the graphical representation of the results are shown in Figure 10 that compare the theoretical to the experimental.

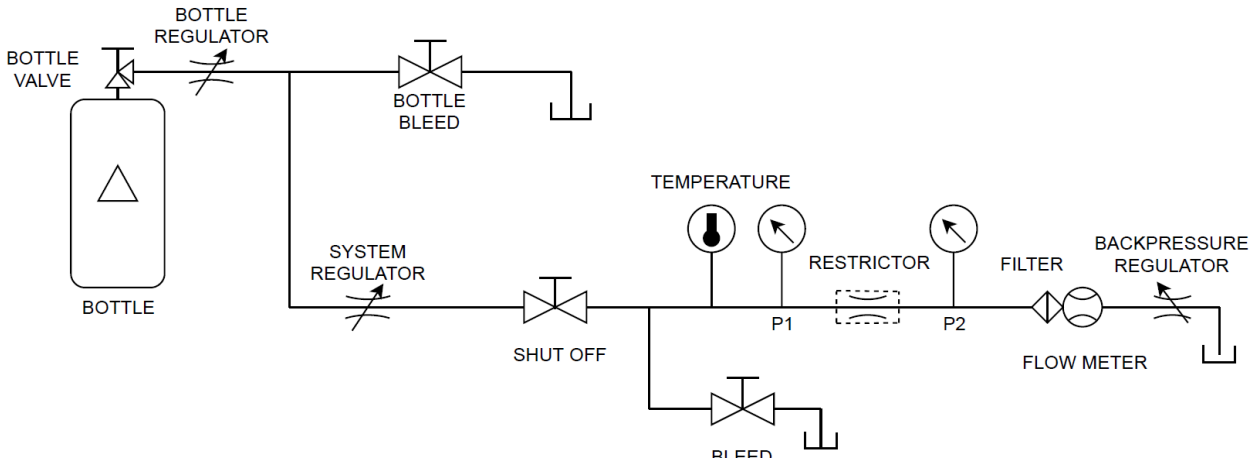

Figure 11: Gas Flow Test Experimental Schematic

Pressure Ratio (P1/P2)	Pressure Ratio (P2/P1)	Pressure (PSIA)		Flow	Test Temperature
		P1	P2	SCCM	°F
6.56	0.153	100.3	15.3	13.19	70.1
5.00	0.200	100	20	13.16	70.2
3.33	0.301	99.8	30	13.13	70.2
2.49	0.402	99.8	40.1	13.07	70.2
1.90	0.527	100	52.65	12.833	70.4
1.66	0.601	99.9	60.06	12.449	70.6
1.42	0.702	99.9	70.12	11.64	70.6
1.25	0.801	99.9	80	9.88	70.7

Table 11: Experimental Pressure Sweep Results (0.0007” Orifice)

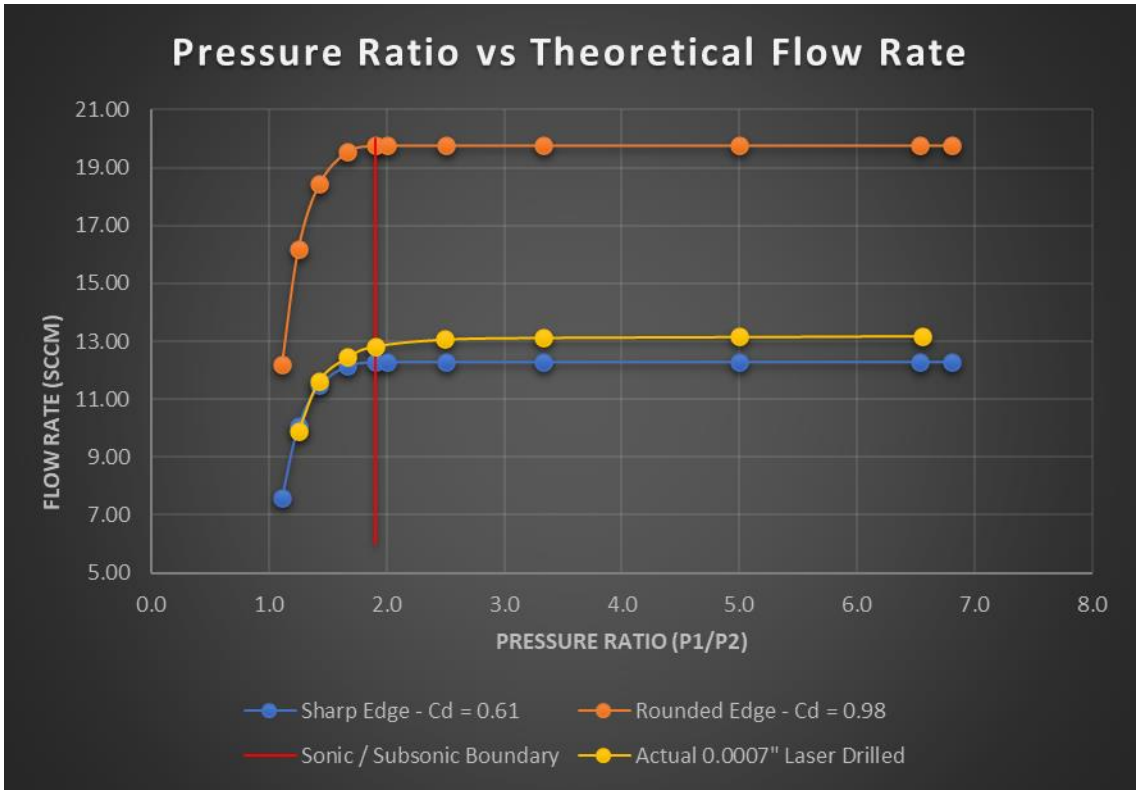

Figure 12: Theoretical vs Experimental Pressure Ratio vs Flow Rate (0.0007" Orifice)

Back calculating, it was found that the discharge coefficient for the laser drilled hole was approximately 0.65. It was shown that using a coefficient of discharge of 0.65 for the theoretical calculations yielded the plot in Figure 10. The percentage difference is much better in the sonic region max of 2.1% at the sonic boundary of 1.9 and under 0.64% for the rest of the sonic region, but the subsonic region then suffers with a maximum of 8.32% and a minimum of 4.05%.

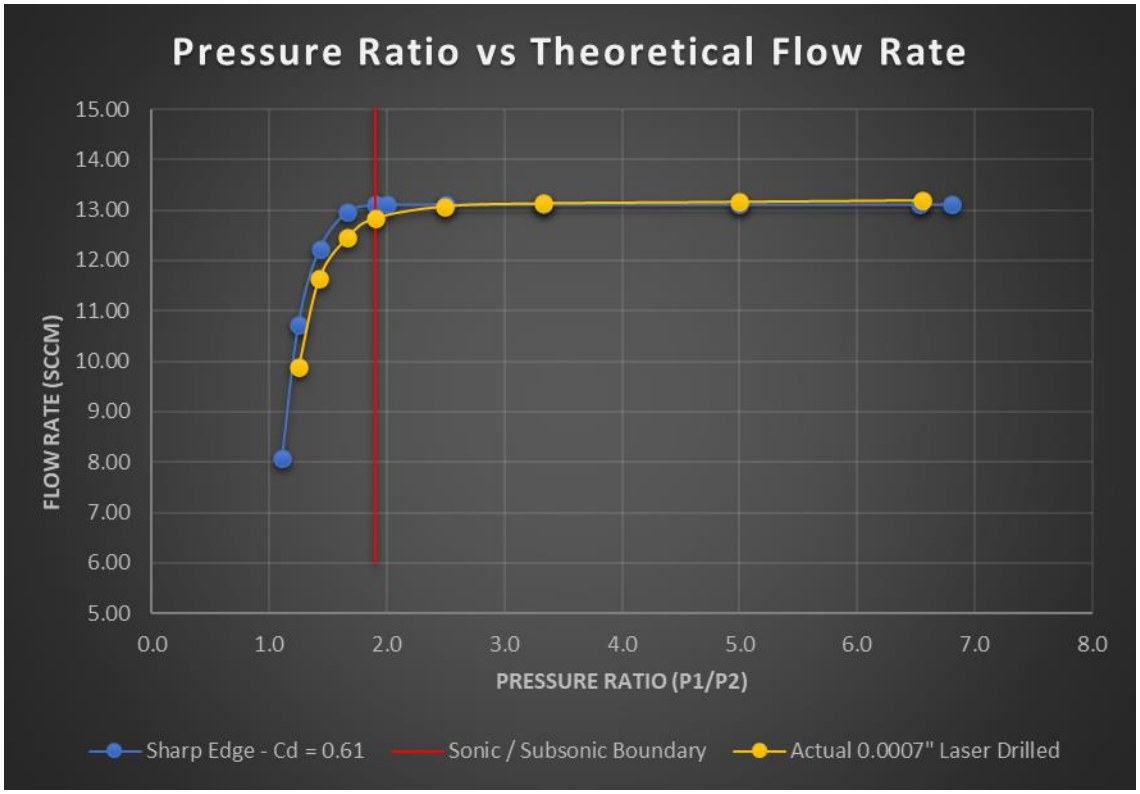

Figure 13: Plot of Experimental vs 0.65 Cd Theoretical

3.7 Single Orifice CFD Validation - Setup

To get to the point of using computation fluid dynamics software for multiple orifices, I first need to ensure my software and model are setup correctly. To do this, I will setup and run a CFD analysis of a single orifice restrictor of the same geometry used in the theoretical and experimental approach.

The software being used is Siemens FloEFD, which works well with SolidWorks models and the interactive layout is just the same. I first modeled the orifice as shown in Figure 12 sandwiched between two tubes with end caps. These are necessary as I am performing an internal flow analysis, so these will mimic the flow tubing used during the experimental flow test.

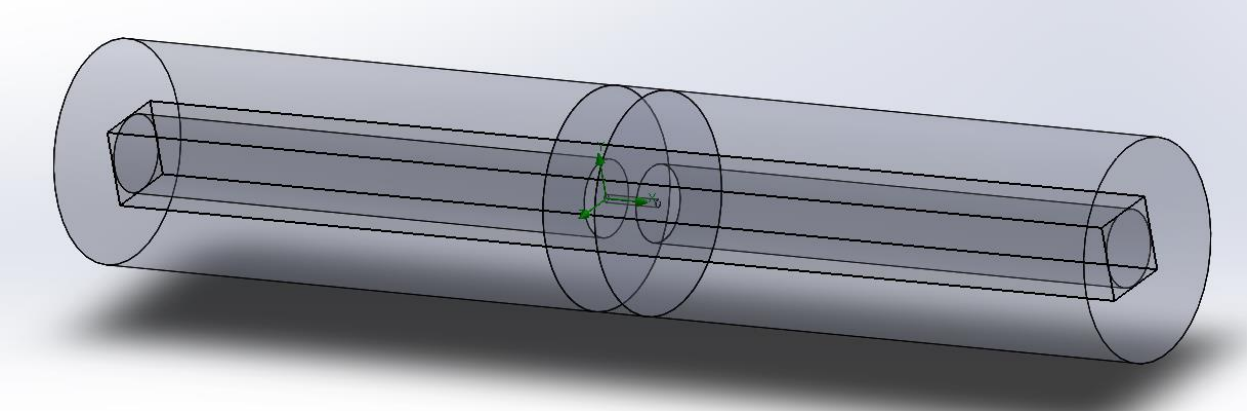

Figure 14: Modeled Orifice and Internal Flow Cavity

It was found through the initial analysis, that inlet was unnecessarily long and increased the computation time due to the increased number of cells in the mesh. Figure 13 shows the model used for analysis.

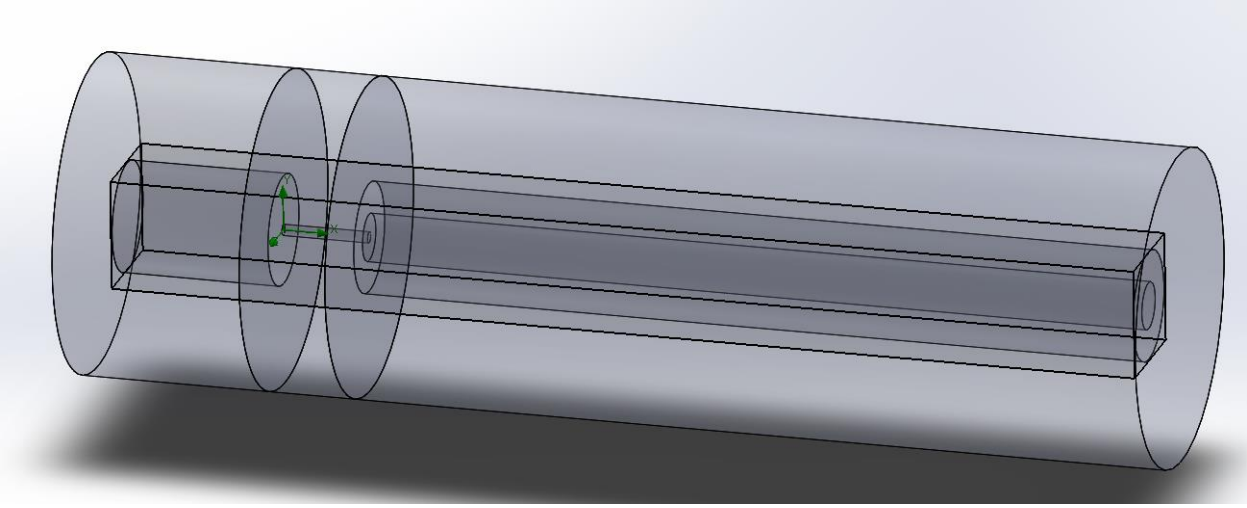

Figure 15: Final Modeled Orifice and Internal Flow Cavity

To start the analysis, the project wizard was set up for an internal analysis type that excluded cavities without flow conditions. Next, the project fluid was selected as Nitrogen with a flow type that considered both laminar and turbulent conditions. Since we are considering an adiabatic and inviscid flow, the wall thermal condition was set to adiabatic and the wall roughness as zero.

Lastly, the initial conditions were set to use the parameters of pressure and temperature and were set at 100 psi and 59°F. The temperature was chosen to be 59°F since that is the standard condition temperature and the pressure was chosen to be 100 psi as this is the inlet pressure used. All general settings can be seen in Figure 14 through Figure 17.

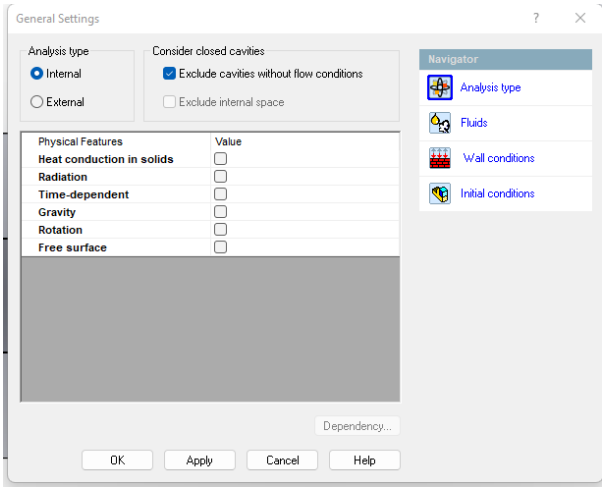

Figure 16: General Settings - Analysis Type

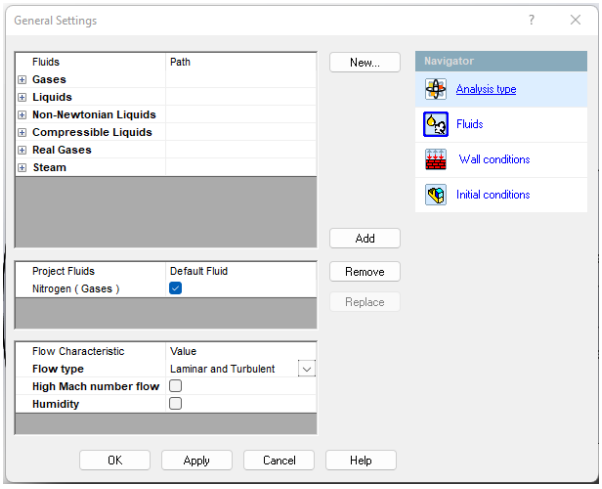

Figure 17: General Settings - Fluids

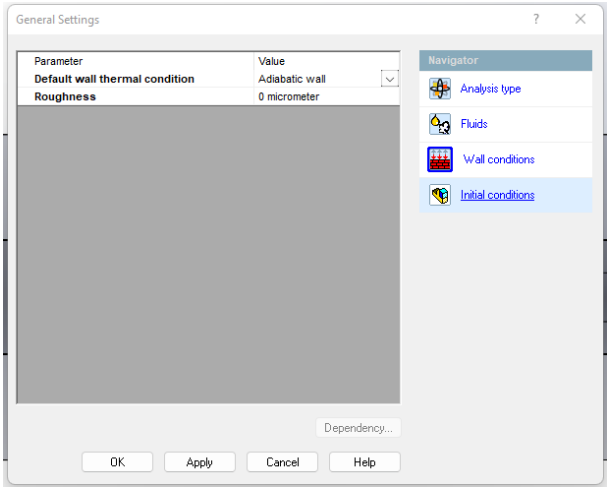

Figure 18: General Settings - Wall Conditions

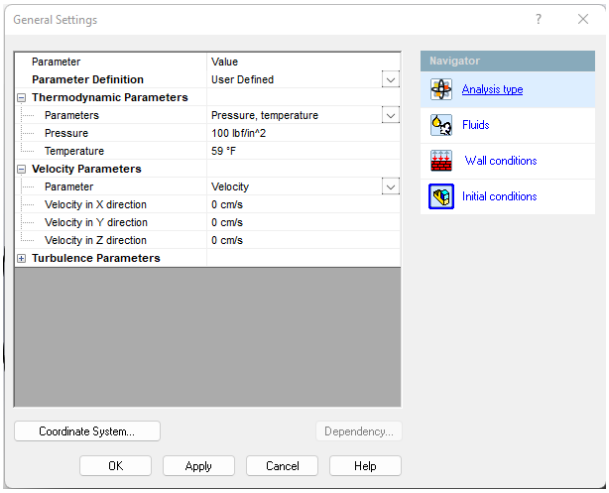

Figure 19: General Settings - Initial Conditions

The computational domain was also set to encompass the internal flow cavities as shown in Figure 18.

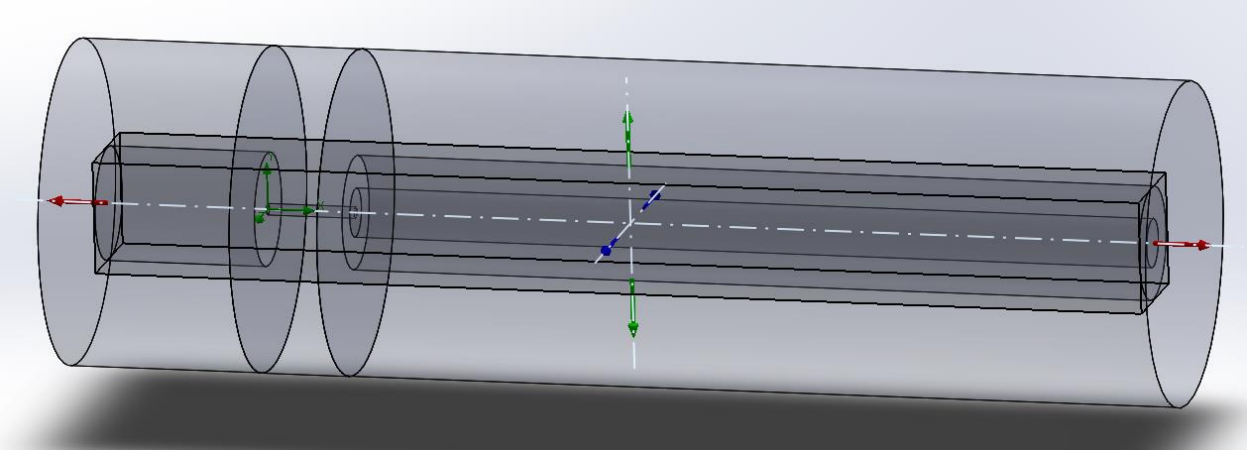

Figure 20: Computational Domain

Next it is necessary to set the boundary conditions. When solving the theoretical and testing the experimental orifice, the upstream and downstream pressures were controlled, and a volumetric flow was output. In the case of this CFD study, the approach had to differ due to the shock waves that would be induced, preventing an accurate depiction of the downstream pressure as well as the changes in density. To counteract this phenomenon and validate my model, I had to approach the analysis in a different way.

Since the volumetric flow is known, I can solve for the mass flow based on the known density of the compressible fluid at the standard conditions of 59°F and 1 atm (14.7 psia), $0.074\ \frac{lb_m}{ft^3} = 1.185\ \frac{kg}{m^3}$. I will use this to be an inlet mass flow with a fixed downstream pressure corresponding to the pressure ratios I desire, and then solve for the upstream pressure. This upstream pressure to downstream pressure ratio should give me the desired pressure ratios to obtain the mass flow. The mass flows used for each point in the units of $\frac{kg}{min}$ are solved by using

$$Volumetric\ Flow\ Rate\ (I) = A * v$$

$$Mass\ Flow\ Rate\ (m) = \rho * I$$

To get the mass flow in the correct units

$$Mass\ Flow\ Rate\ \left(\frac{kg}{min}\right) = \frac{\rho * I}{100^3}$$

The resultant mass flow rates can be shown in Table 12.

Pressure Ratio	**P1 (PSIA)**	**P2 (PSIA)**	**Volumetric Flow (SCCM)**	**Mass Flow (kg/min)**
6.54	100	15.3	13.19	1.5636×10^{-5}
5.00		20	13.16	1.5600×10^{-5}
3.33		30	13.13	1.5564×10^{-5}
2.50		40	13.07	1.5493×10^{-5}
1.90		52.63	12.83	1.5212×10^{-5}
1.67		60	12.45	1.4757×10^{-5}
1.43		70	11.64	1.3798×10^{-5}
1.25		80	9.88	1.1171×10^{-5}

Table 12: Mass Flow Calculations for CFD Input

The mass flows calculated were used as a uniform inlet mass flow coming from the inlet surface as shown in Figure 19. The outlet was set at the far end of the flow cavity surface as shown in Figure 20. To validate the process, the inlet pressure should come in at 100 psi for all flow rates and corresponding downstream pressures. To confirm this, the total pressure at the inlet surface was used at the goal and used for analysis convergence control as seen in Figure 21. Since the

experimental results were collected at 70°F, the fluid was set at this temperature for all boundary conditions.

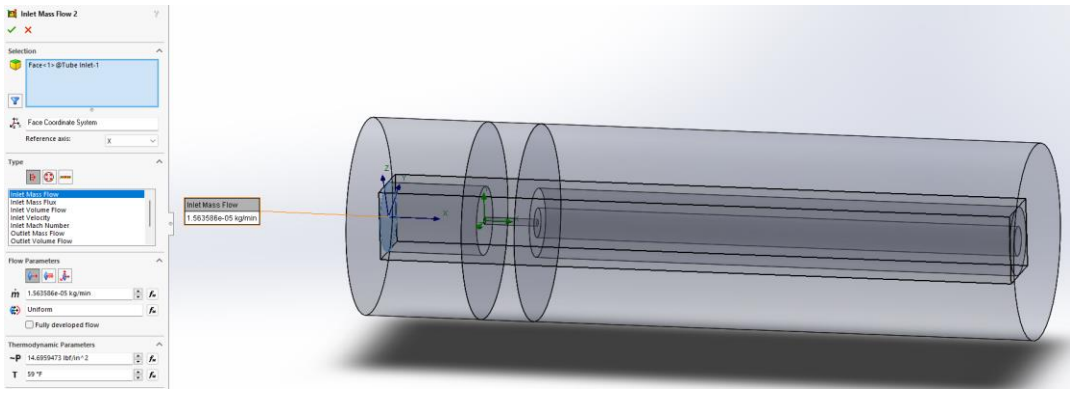

Figure 21: Inlet Mass Flow Condition

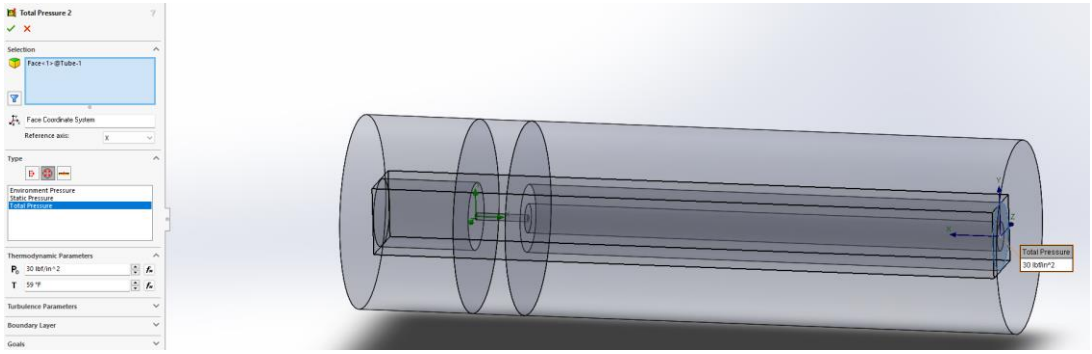

Figure 22: Outlet Total Pressure Condition

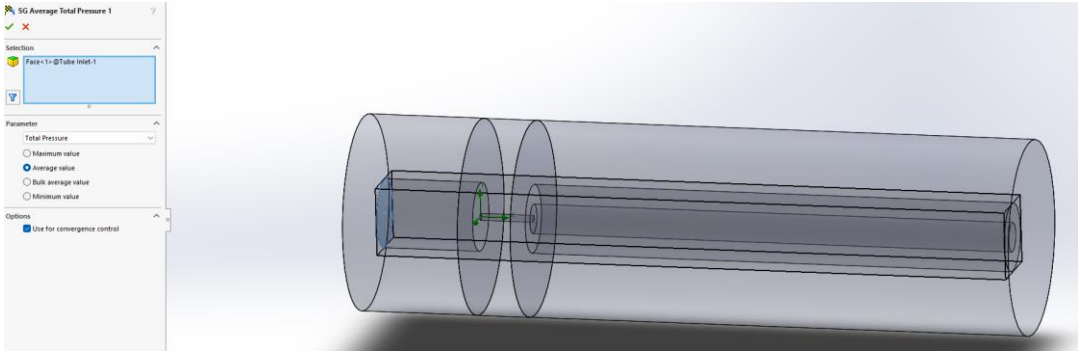

Figure 23: Inlet Total Pressure Surface Goal

3.8 Single Orifice CFD Validation – Mesh Convergence Study

Next, is the mesh optimization and convergence study. This is an important step in any CFD analysis, as having a mesh that is not optimized could impact the value obtained for the inlet pressure. FloEFD has a user-friendly global mesh "slider" that uses an arbitrary number which increases the mesh refinement automatically. There is also the ability to create local meshes in areas where more refinement and resolution is needed.

To start the convergence study, I start with the number "1" on the global mesh slider as shown in Figure 22. I also identify the smallest gap in the model which equates to the 0.0007-inch orifice (0.001778 cm).

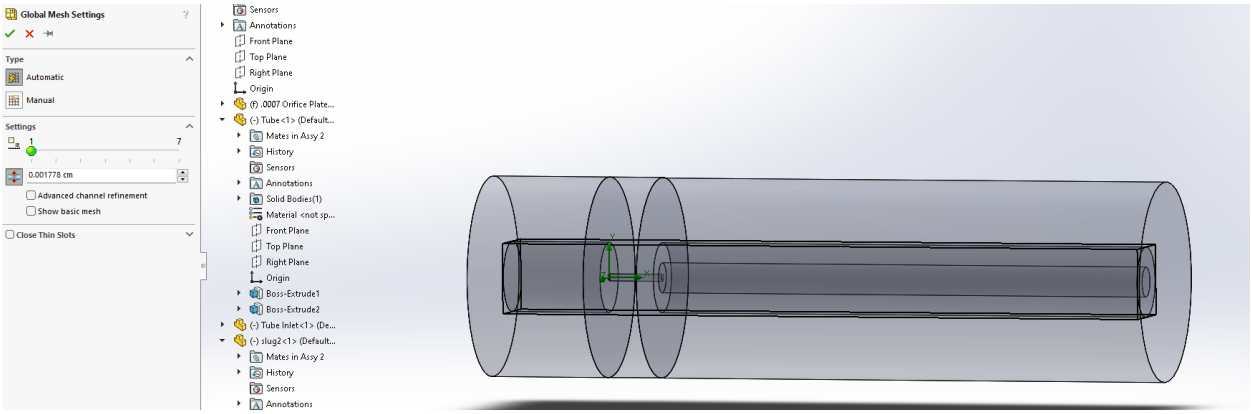

Figure 24: Global Mesh Slider = 1

Running the flow analysis automatically solves for the mesh and upstream pressure goal. After the solver finishes, a summary of data is generated which shows that for this analysis, the total fluid cells was equal to 2,082 and there contained 1,414 fluid cells that contacted a solid surface. The analysis went through 75 iterations upon convergence which equated to 1.875 travels where 1 travel means that the analysis made it from one side of the internal cavity to the other, so a full

cycle through all the cells. The computation time to complete this analysis is shown as 8 seconds. All this information is re-iterated in Figure 23. The mesh is also shown in Figure 24 which is a cut plot of the front plane of the model.

Parameter	Value
Status	Solver is finished.
Total cells	2,082
Fluid cells	2,082
Fluid cells contacting solids	1,414
Iterations	75
Last iteration finished	07:47:47
CPU time per last iteration	00:00:00
Travels	1.875
Iterations per 1 travel	41
Cpu time	0 : 0 : 8
Calculation time left	0 : 0 : 0
Run at	NAVINI-LPT
Number of cores	24

Figure 25: Global Mesh Slider = 1 Analysis Summary

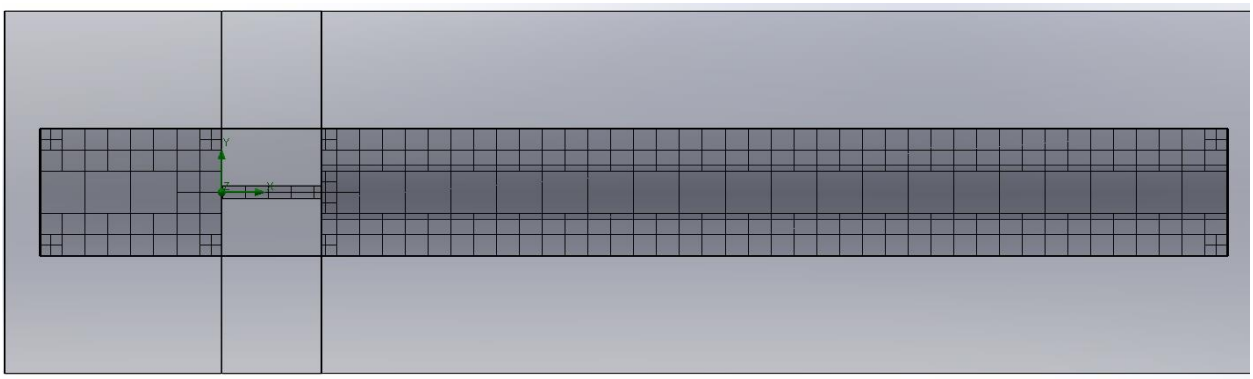

Figure 26: Global Mesh Slider = 1 Mesh Cut Plot (Front Plane)

The solver found P1 to be 387.64 psia which is approximately 118% difference from the desired result of 100 psia. It is seen that this could be due to the coarse mesh used. The auto mesh did refine more around the smaller passage as well as the outer walls, but not enough to obtain an accurate answer.

For the convergence study, the global mesh slider was run at each increment from 1 – 7. The cut plots of the meshes can be seen in Figure 25 through Figure 32. The number of fluid cell values and calculation times for each increment are shown in Table 13.

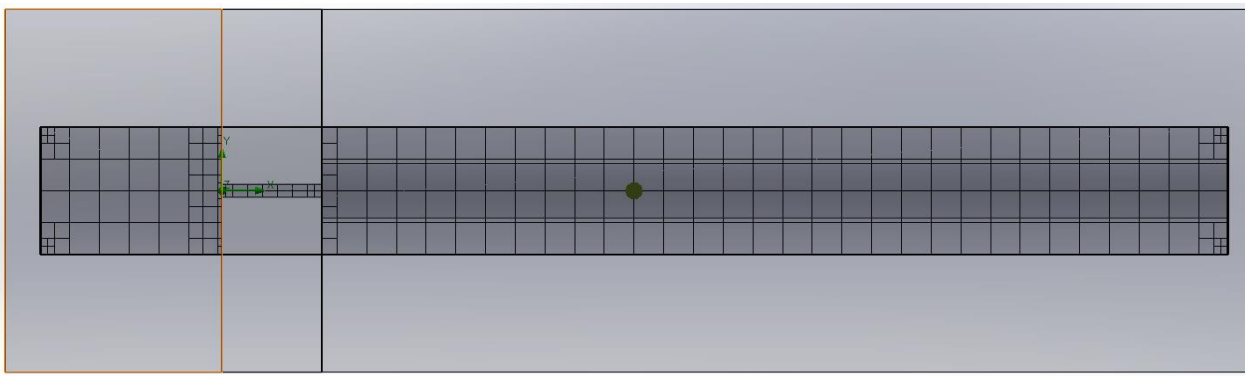

Figure 27: Global Mesh Slider = 2 Mesh Cut Plot (Front Plane)

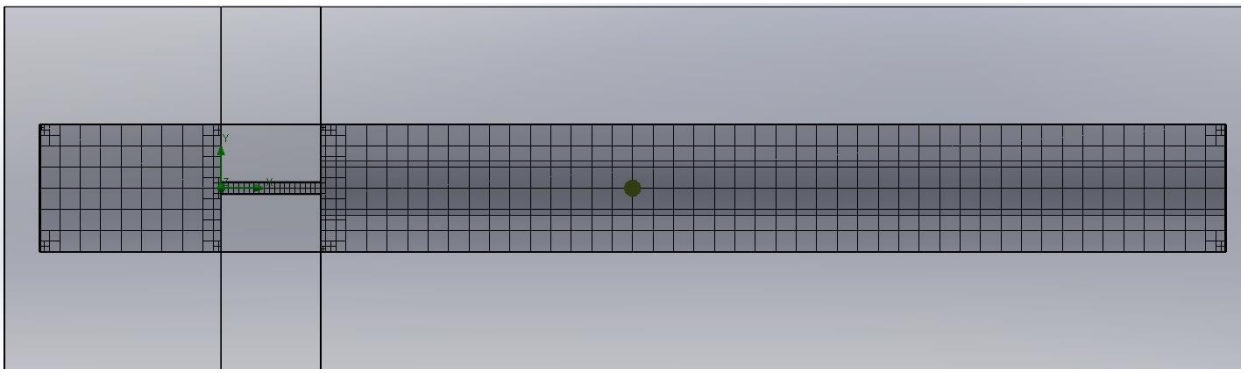

Figure 28: Global Mesh Slider = 3 Mesh Cut Plot (Front Plane)

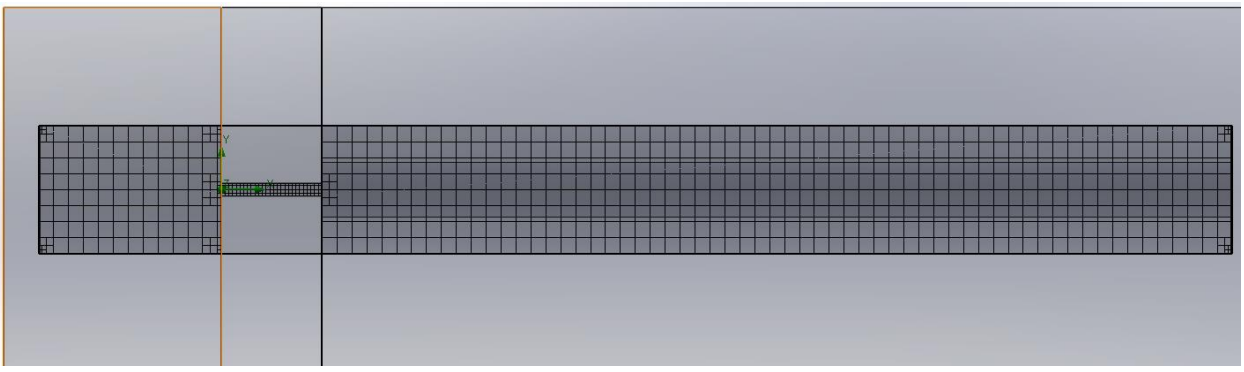

Figure 29: Global Mesh Slider = 4 Mesh Cut Plot (Front Plane)

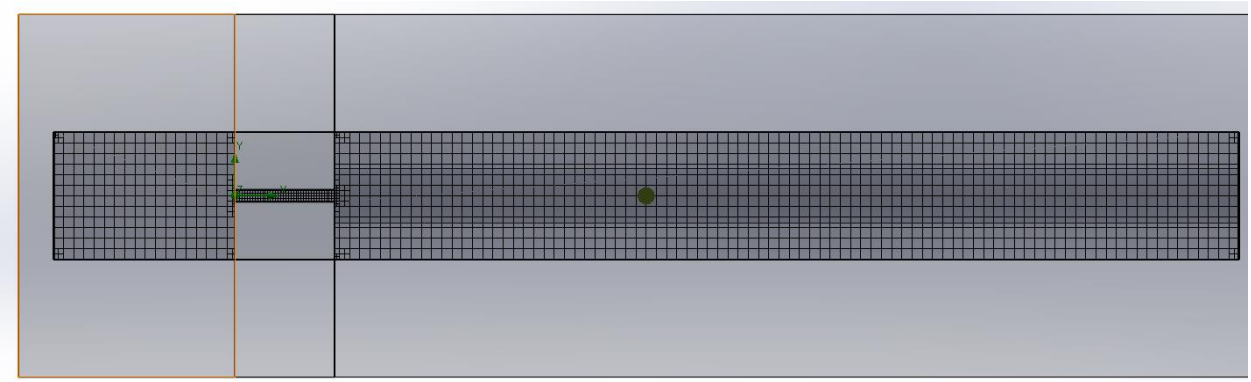

Figure 30: Global Mesh Slider = 5 Mesh Cut Plot (Front Plane)

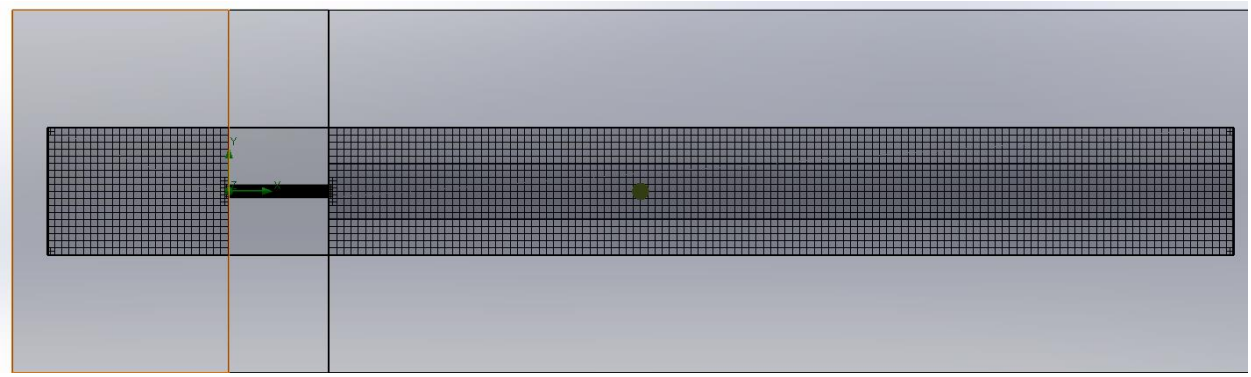

Figure 31: Global Mesh Slider = 6 Mesh Cut Plot (Front Plane)

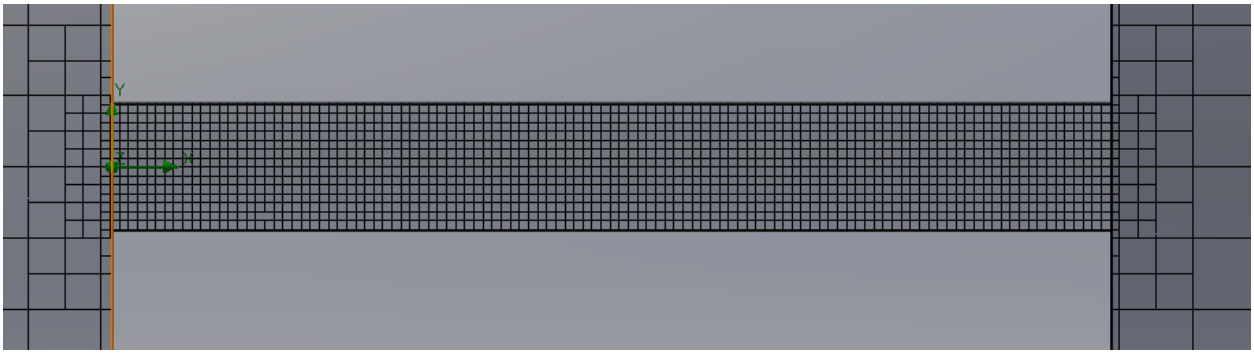

Figure 32: Global Mesh Slider = 6 Mesh Cut Plot (Orifice View)

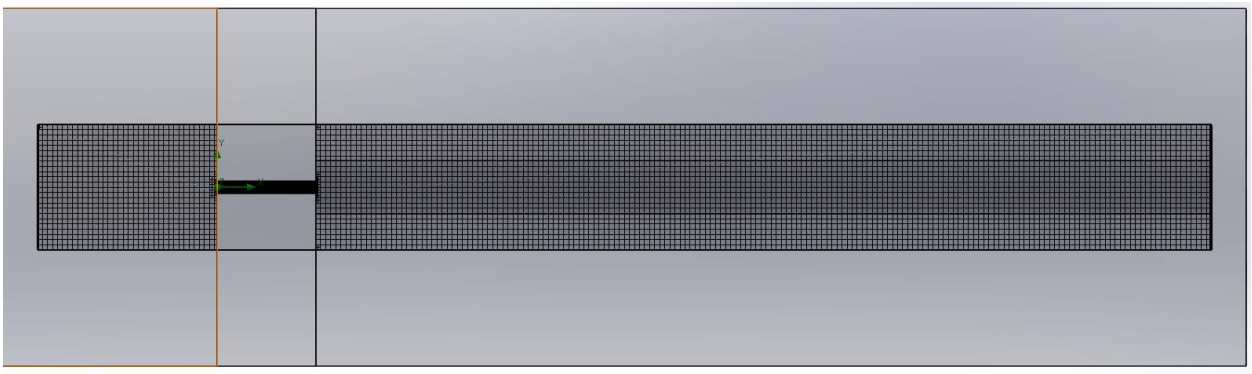

Figure 33: Global Mesh Slider = 7 Mesh Cut Plot (Front Plane)

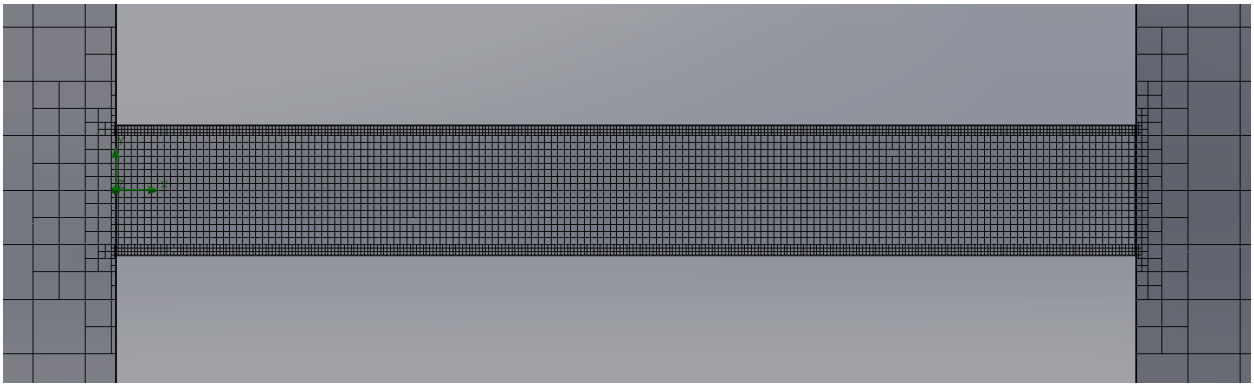

Figure 34: Global Mesh Slider = 7 Mesh Cut Plot (Orifice View)

Global Slider	Mesh Cells	P1 (PSIA)	CPU Time (sec)	Percent Difference from Actual
1	2082	387.64	8	118.0
2	1460	218.9	5	74.6
3	4352	116.17	7	15.0
4	6736	122.23	7	20.0
5	17020	113.36	16	12.5
6	65872	109.73	41	9.3
7	250722	107.65	182	7.4

Table 13: Global Mesh Slider Data Summary

As we can see, the global mesh slider increases the number of cells which also increases the computation time, but the value of P1 looks like it is starting to converge to a value. It can be seen from the increasing mesh, that the convergence is becoming more apparent as the mesh through the orifice and around the entry and exit of the orifice becomes more refined. It is also seen from

a cut plot of the velocity (Figure 33), there is a jet stream formed in the center of the outlet tube, so it would be advantageous to capture this.

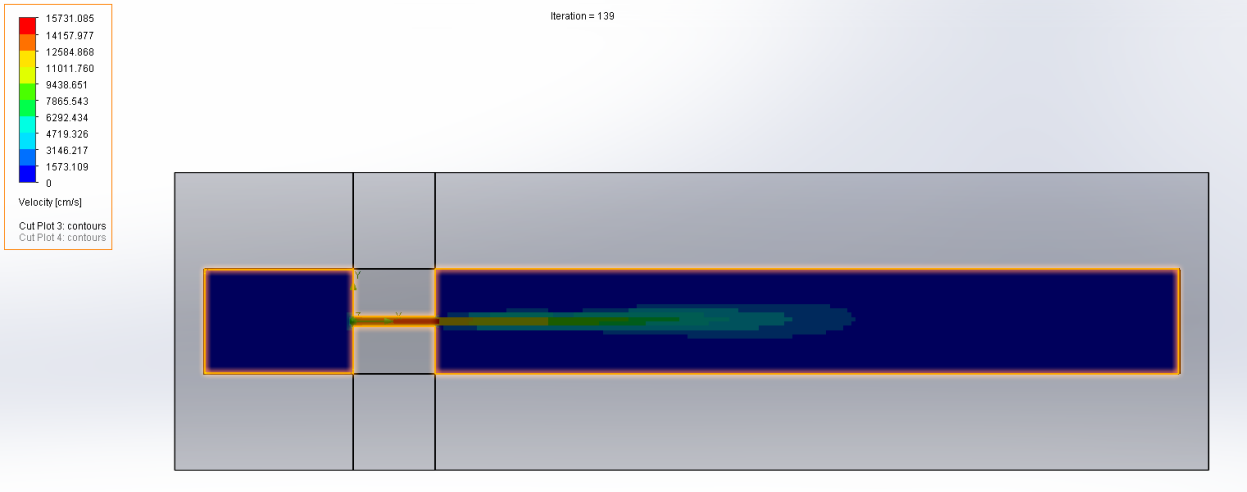

Figure 35: Velocity Cut Plot Jet Stream

To capture more of the orifice and the jet stream, local meshes can be utilized to optimize the mesh cells where the analysis capturing is more important. A local mesh is first made in just the orifice. The settings of the refinement can be see in Figure 34.

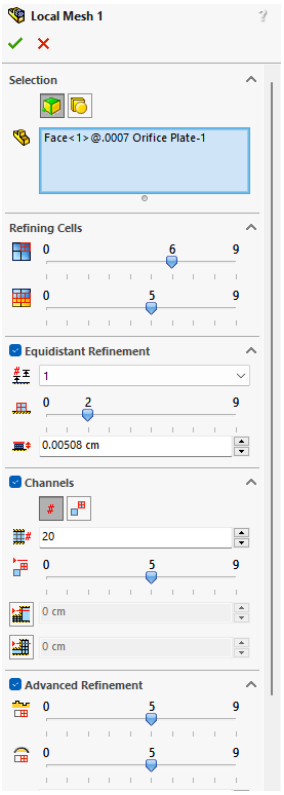

Figure 36: Orifice Local Mesh Refinement

The mesh was run with the global mesh slider at level 4 and the resulting mesh cut plot and summary data was generated. The inlet and outlet of the orifice is more refined as well as the internal walls and center of the orifice.

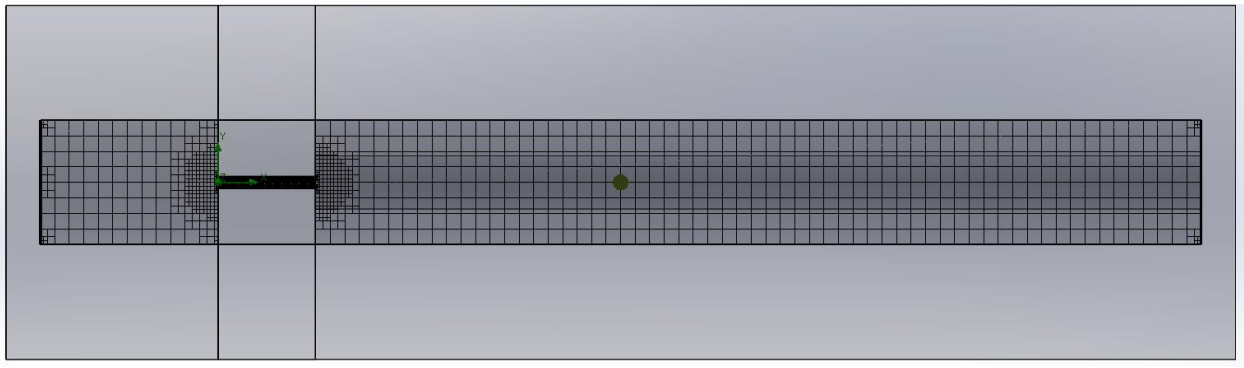

Figure 37: Orifice Local Mesh and Global Mesh Slider = 4 Cut Plot (Front Plane)

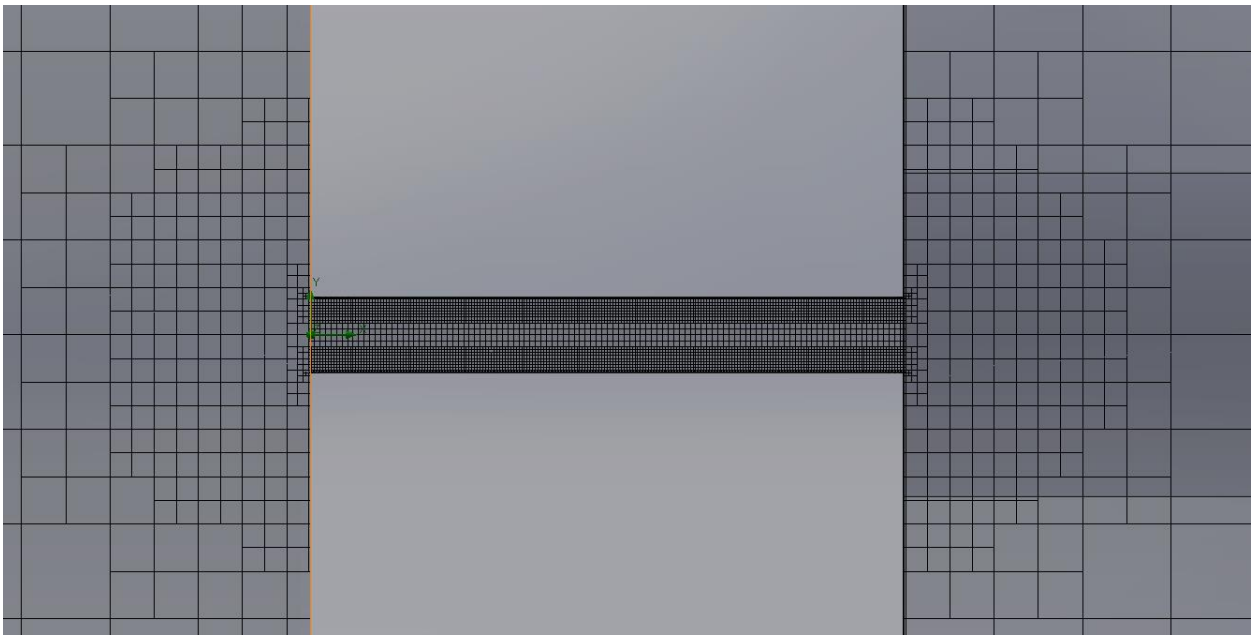

Figure 38: Orifice Local Mesh and Global Mesh Slider = 4 Cut Plot (Orifice View)

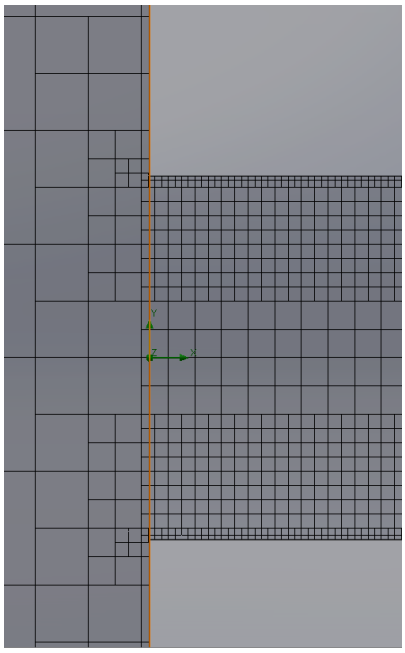

Figure 39: Orifice Local Mesh (Zoomed)

To capture the potential jet stream at the exit of the orifice to the outlet of the outlet tube, a small diameter slug was inserted and suppressed in the flow analysis, but a local mesh was generated in the geometry that it occupies.

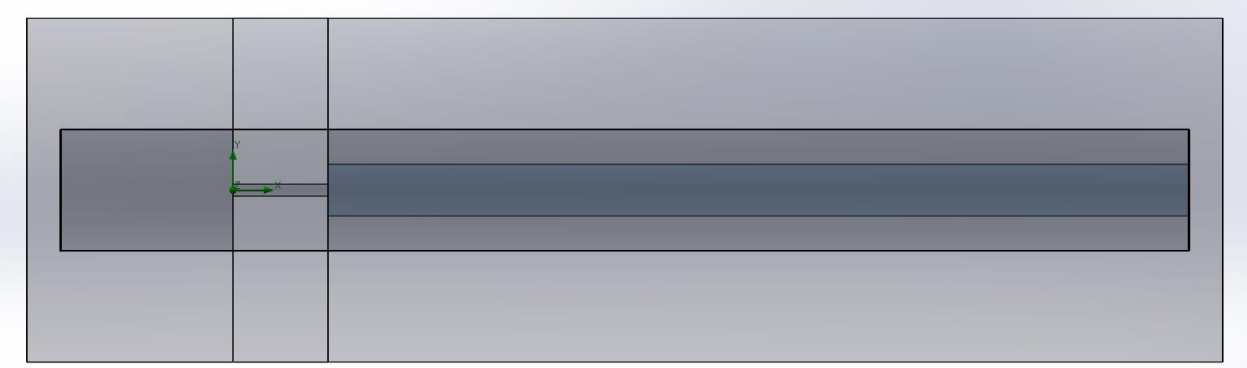

Figure 40: Outlet Slug Geometry to Capture Jet Stream

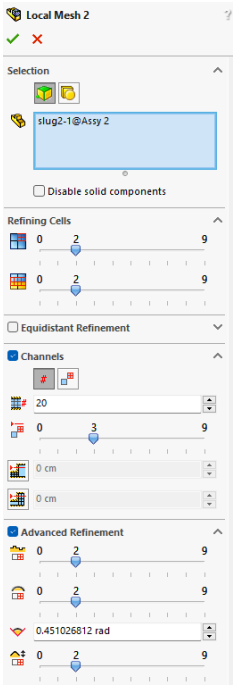

Figure 41: Slug Local Mesh Refinement

The local mesh was run with the global mesh slider level of 4 and 5 with the orifice local mesh unsuppressed.

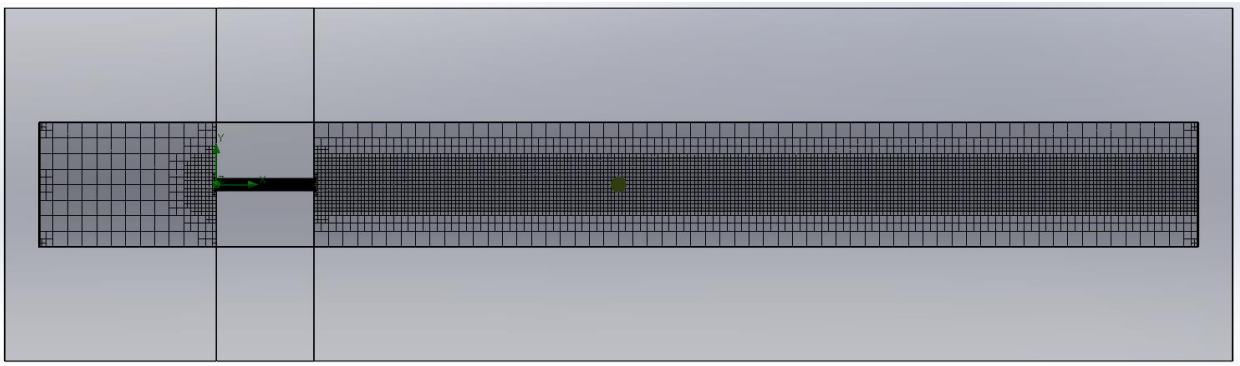

Figure 42: Slug and Orifice Local Mesh, Global Mesh = 4

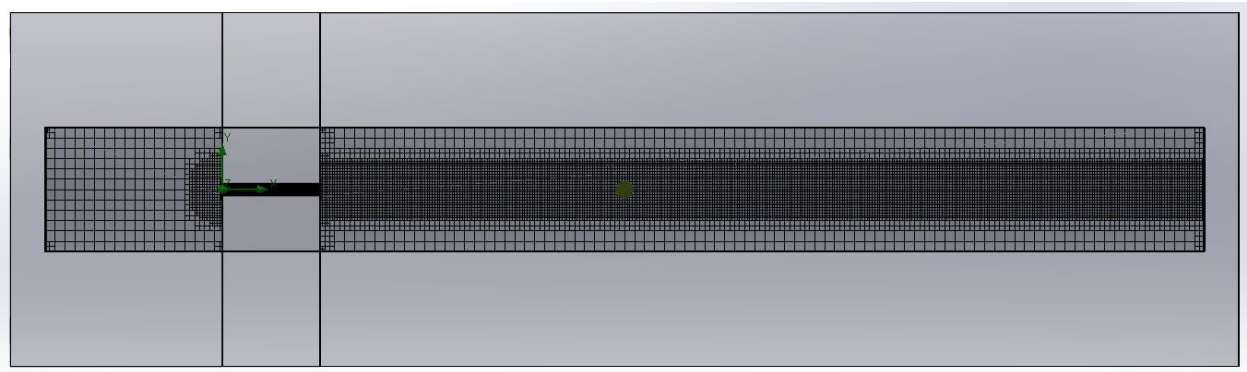

Figure 43: Slug and Orifice Local Mesh, Global Mesh = 5

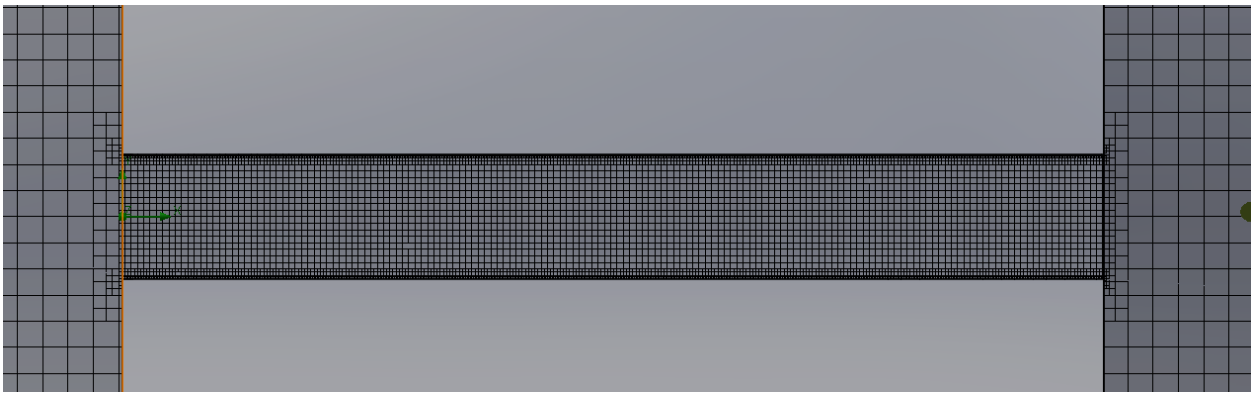

Figure 44: Slug and Orifice Local Mesh, Global Mesh = 5 (Orifice View)

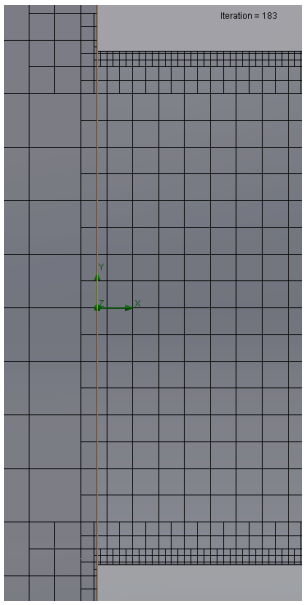

Figure 45: Slug and Orifice Local Mesh, Global Mesh = 5 (Orifice View Zoomed)

The summary data using local meshes can be seen in Table 14 where local mesh 1 refers to the orifice local mesh and local mesh 2 refers to the slug local mesh.

Global Slider	Local Mesh	Mesh Cells	P1 (PSIA)	CPU Time (sec)	Percent Difference from Actual
4	1	259688	107.81	189	7.5
4	1 &2	322352	107.8	255	7.5
5	1&2	642380	107.68	632	7.4

Table 14: Local Mesh and Global Mesh Data Summary

Combining all the summary data, we can make a convergence plot that compares the average P1 value to the number of total cells for the mesh as shown in Figure 44.

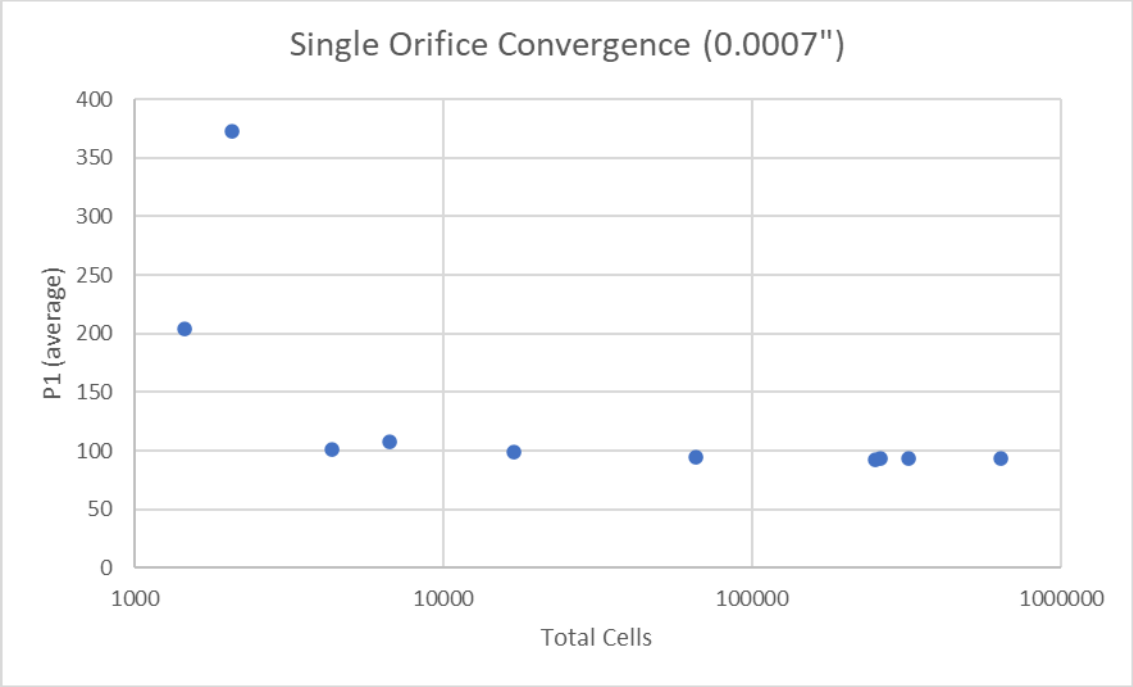

Figure 46: Single Orifice Convergence Plot

This plot shows that the convergence of the P1 value occurs starting around 17,000 cells, but truly converges with a percent difference of around 7.4% which occurs around 250,000 cells. We can see that with the increased number of cells, we have increased computation time. Using local mesh 1 and 2 with a global slider of 4 seems to be the best balance between convergence and CPU time. Going to global mesh slider level of 5 with both local meshes doubles the mesh cells and CPU time but yields the same result. Turning off mesh 2 reduces the CPU time, but only by one minute, which is relatively low time. Using the global slide level 4 with both local meshes will be the most advantageous mesh settings due to the time required to compute and the mesh refinement.

3.9 Single Orifice CFD Validation – Parametric Study

Now that the general settings have been defined and the mesh optimized using a convergence study, we now move to validate the single orifice at all points tested in the sonic and subsonic regions. This is conducted using a parametric study which allows the use of multiple design points to study a variety of inputs. To validate, a design point was made for each mass flow rate with the corresponding downstream pressure as shown in Figure 45. Note that total downstream pressure has 14.7 psi added to ensure we are in psia.

Summary	Design Point 1	* Design Point 2	* Design Point 3	* Design Point 4	* Design Point 5	* Design Point 6	* Design Point 7	* Design Point 8
Mass flow rate (Inlet Mass Flow 2) [kg/min]	1.563586e-05	1.56003e-05	1.556474e-05	1.549361e-05	1.521266e-05	1.475746e-05	1.379844e-05	1.171208e-05
Total Pressure (Total Pressure 2) [lbf/in^2]	30	34.7	44.7	54.8	67.35	74.86	84.82	94.7

Figure 47: Single Orifice Parametric Study Design Points

Running the analysis yielded the results listed in Table 15. Figure 46 displays the curve obtained via CFD compared to the values obtained using theoretical and experimental analysis.

Pressure Ratio (P1/P2)	Pressure (PSIA)		Flow	Test Temperature
	P1	P2	SCCM	°F
6.15	94.2	15.3	13.19	70.1
4.84	96.8	20	13.16	70.2
3.28	98.4	30	13.13	70.2
2.51	100.8	40.1	13.07	70.2
1.94	102.3	52.65	12.833	70.4
1.74	104.7	60.06	12.449	70.6
1.51	106.1	70.12	11.64	70.6
1.35	108	80	9.88	70.7

Table 15: Single Orifice Parametric Study Results

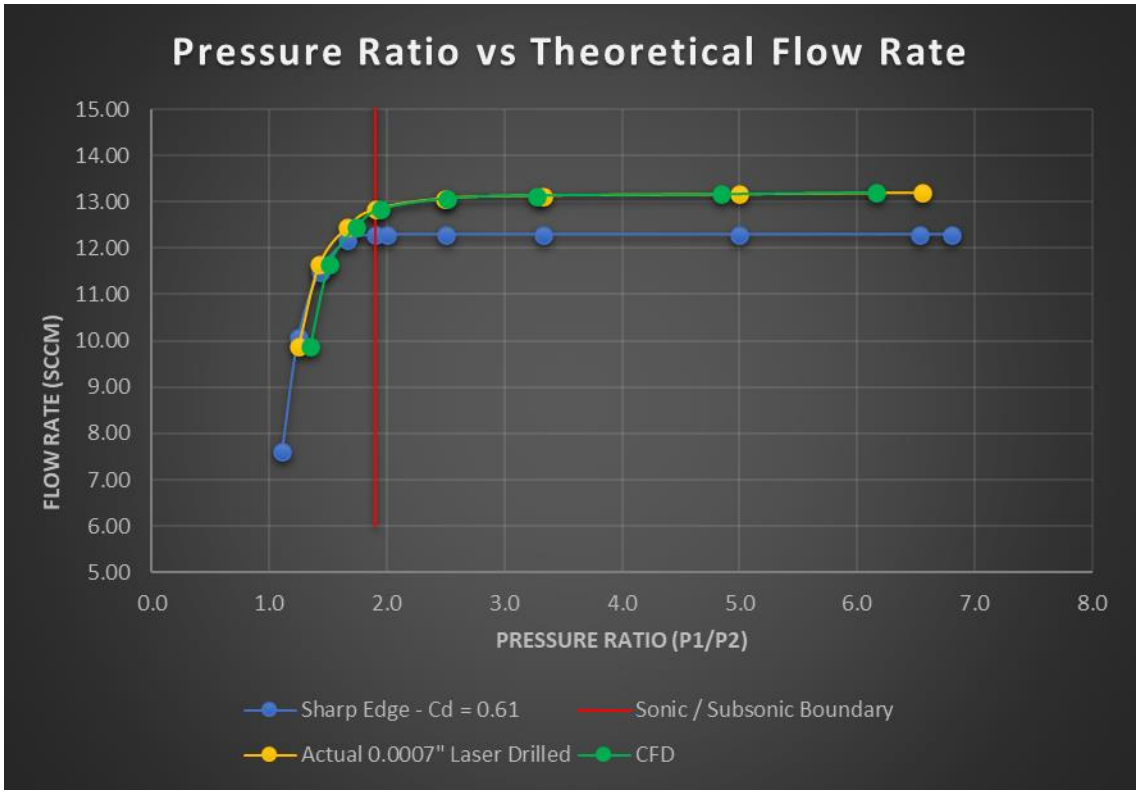

Figure 48: Single Orifice Parametric Study Plot vs Theoretical and Experimental

As we can see, the curve fits closely to the actual experimental data as expected. Some of the points are off a bit at the higher-pressure ratios, but the most important characteristic of the constant mass flow in the sonic region following the law of forbidden signals [6]. We obtain fairly accurate flow results at the lower pressure ratios in the subsonic region.

With the information collected, we can safely say that the CFD analysis validated setup and optimization of the single orifice element as calculated theoretically and testing empirically. With this information, we can investigate multiple orifices in series to examine what the impact is on the intermediate pressure of the two orifices as the orifice ratios vary.

3.10 Multi-Orifices in Series and Intermediate Pressure - Setup

To start the analysis of the multi-orifice restrictors a model is made similar to the single orifice but doubled. The outlet from the first orifice is sufficiently long as to not allow the formation of the jet to run directly into the next orifice. The multi-orifice model can be seen in Figure 47 with a schematic depiction in Figure 48.

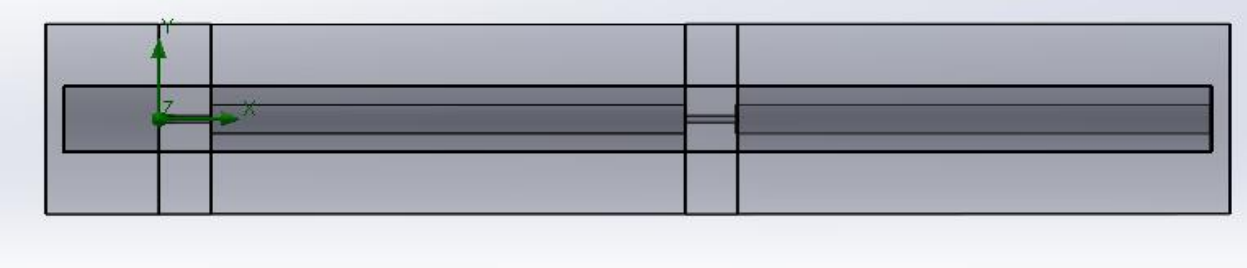

Figure 49: Multi-Orifice in Series Model

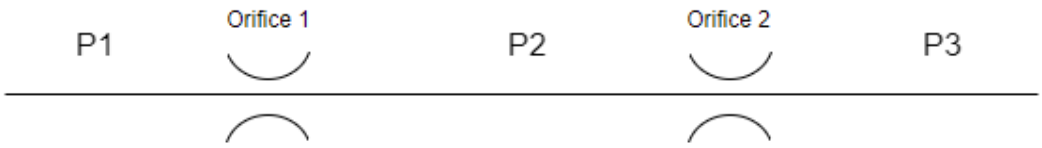

Figure 50: Multi-Orifice in Series Schematic

The setup is the same as for the single orifice for all the general settings including the wall conditions, the fluids, the flow characteristics, and the initial conditions. The inlet flows and outlet total pressure used for boundary conditions are the same as used in Table 12 for the single orifice restrictor. To study the intermediate pressure, another surface goal is added, which solves for the total pressure at the inlet of the second orifice as shown in Figure 48 and 49 highlighted in blue.

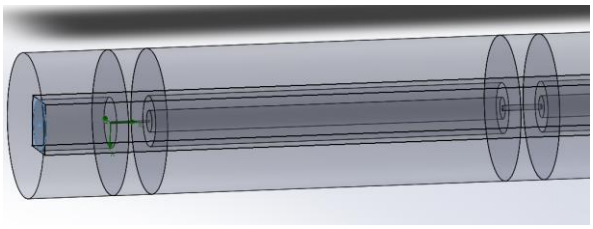

Figure 51: Inlet Surface Goal - Multi-Orifice

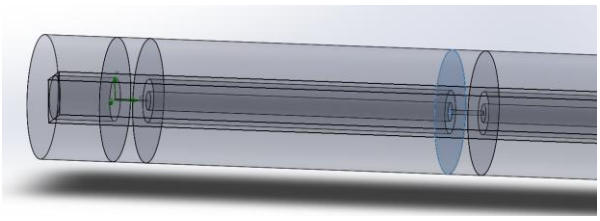

Figure 52: Intermediate Pressure Surface Goal - Multi-Orifice

To start, a mesh convergence was performed which optimized similar to the single orifice since the orifices in series are a replica of the single orifice. Two additional local meshes were created at the second orifice and at the outlet of the second orifice to capture the jet stream occurring downstream.

To study the intermediate pressure based on the orifice restriction ratio, the first orifice was made into five different configurations as shown in Table 16 where 0.0007 is used as the downstream orifice size for each case, which equates to a restriction of 2,105,939. To find the hole sizes for the restriction ratios, we use the coefficient of discharge found of 0.65 in equation 35 is used which simplifies the restriction and allows to solve for a hole diameter for the restriction ratios

$$\Omega = \frac{1.03191}{D^2} \tag{35}$$

Restriction Ratio	Hole Size (in)	Restriction
0.5	0.000990	1052969
1	0.000700	2105939
2	0.000495	4211878
4	0.000350	8423755
10	0.000221	21059388

Table 16: Restriction Ratio Orifice Configurations

3.11 Multi-Orifices in Series and Pressure Ratio Impact

As to not disrupt the flow of analysis, all cut plots for the following parametric studies showing the pressure and velocity through the model can be found in the Appendix.

Starting with the restriction ratio of 0.5, the upstream orifice size was increased to 0.00099 inches while the downstream orifice was kept static at 0.0007 inches. The parametric study was used to run through eight design points that utilized the uniform inlet mass flow and outlet total pressures as described in Table 12. The resulting inlet total pressure and intermediate total pressures were solved for. It is seen that the pressure drop across the first larger orifice (less restriction) has a much smaller pressure drop across the orifice as well as a much lower velocity in the orifice and expanding out of the orifice. The second hole is where most of the pressure drop and high velocity is seen, showing the sonic conditions at that point for the higher-pressure ratios. The first orifice is never sonic as expected since the hole size is large in comparison to the secondar orifice.

With the restriction ratio of 1, both orifices are 0.0007 inches in diameter. In all cases for this parametric study, the first orifice is subsonic as the second orifice is sonic for most of the higher-pressure ratios and then goes subsonic. The rest of the configurations utilize a larger restriction ratio ranging from 2 to 10. Each of these instances in the parametric study exhibit a sonic condition at both orifices in many instances, but most of the sonic conditions are across the first orifice as expected since the restriction is higher resulting in a higher pressure drop. Table 17 shows the sonic and subsonic conditions for all design points run. Green cells are sonic and red cells are subsonic.

Restriction Ratio	P1	P2	P3	P1/P3	P1/P2	P2/P3
0.5	83.85	77.39	15.30	5.48	1.08	5.06
	83.80	77.37	20.00	4.19	1.08	3.87
	85.55	79.25	30.00	2.85	1.08	2.64
	87.08	80.95	40.10	2.17	1.08	2.02
	91.32	85.67	52.65	1.73	1.07	1.63
	93.75	88.53	60.16	1.56	1.06	1.47
	97.04	92.56	70.12	1.38	1.05	1.32
	98.60	95.28	80.00	1.23	1.03	1.19
1	104.06	78.26	15.30	6.80	1.33	5.12
	103.89	78.18	20.00	5.19	1.33	3.91
	104.24	78.81	30.00	3.47	1.32	2.63
	105.66	81.13	40.10	2.64	1.30	2.02
	108.47	85.78	52.65	2.06	1.26	1.63
	109.60	88.65	60.16	1.82	1.24	1.47
	110.65	92.66	70.12	1.58	1.19	1.32
	108.65	95.35	80.00	1.36	1.14	1.19
2	176.41	78.19	15.30	11.53	2.26	5.11
	176.05	78.18	20.00	8.80	2.25	3.91
	176.82	80.04	30.00	5.89	2.21	2.67
	175.95	81.69	40.10	4.39	2.15	2.04
	174.40	86.35	52.65	3.31	2.02	1.64
	171.09	89.23	60.16	2.84	1.92	1.48
	164.31	93.13	70.12	2.34	1.76	1.33
	149.08	95.72	80.00	1.86	1.56	1.20
4	359.75	78.56	15.30	23.51	4.58	5.13
	358.84	78.53	20.00	17.94	4.57	3.93
	363.09	81.78	30.00	12.10	4.44	2.73
	356.30	82.18	40.10	8.89	4.34	2.05
	350.10	87.02	52.65	6.65	4.02	1.65
	340.60	90.03	60.16	5.66	3.78	1.50
	320.90	94.21	70.12	4.58	3.41	1.34
	276.73	96.90	80.00	3.46	2.86	1.21
10	807.57	68.01	15.30	52.78	11.87	4.45
	805.65	68.10	20.00	40.28	11.83	3.40
	936.19	83.81	30.00	31.21	11.17	2.79
	799.85	74.22	40.10	19.95	10.78	1.85
	785.58	81.01	52.65	14.92	9.70	1.54
	762.50	84.93	60.16	12.67	8.98	1.41
	773.81	89.15	70.12	11.04	8.68	1.27
	670.56	96.00	80.00	8.38	6.98	1.20

Table 17: Sonic/Subsonic Values Through Multi-Orifices in Series

3.12 Multi-Orifices in Series and Intermediate Pressure

When faced with orifices in series, it is advantageous to solve for the intermediate pressures since with compressible fluid flow, there is an uneven pressure drop across the orifices. In the case of two orifices, the data collected gives a value of the intermediate pressure, $P2$, as a percentage of the upstream pressure, $P1$, when compared to different pressure ratios of the inlet upstream pressure and the outlet downstream pressure, $\frac{P1}{P3}$. The graphic in Figure 51 shows curves for each restriction ratio and the resulting intermediate pressure as a percentage of the upstream pressure.

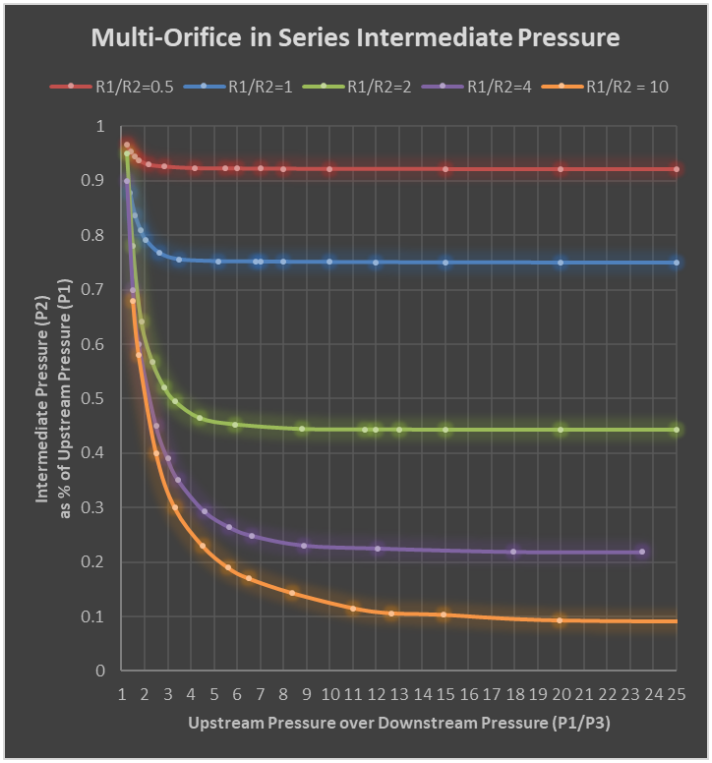

Figure 53: Overall Pressure Ratio (P1/P3) vs Intermediate Pressure as % of P1

When comparing to the orifices in series graphic in the Lee Hydraulic Manual [6] which was calculated theoretically, we can see that the curves match well, but are more off when the curves

are horizontal at the lower restriction ratios. The comparison can be seen in Figure 52 and Table 18.

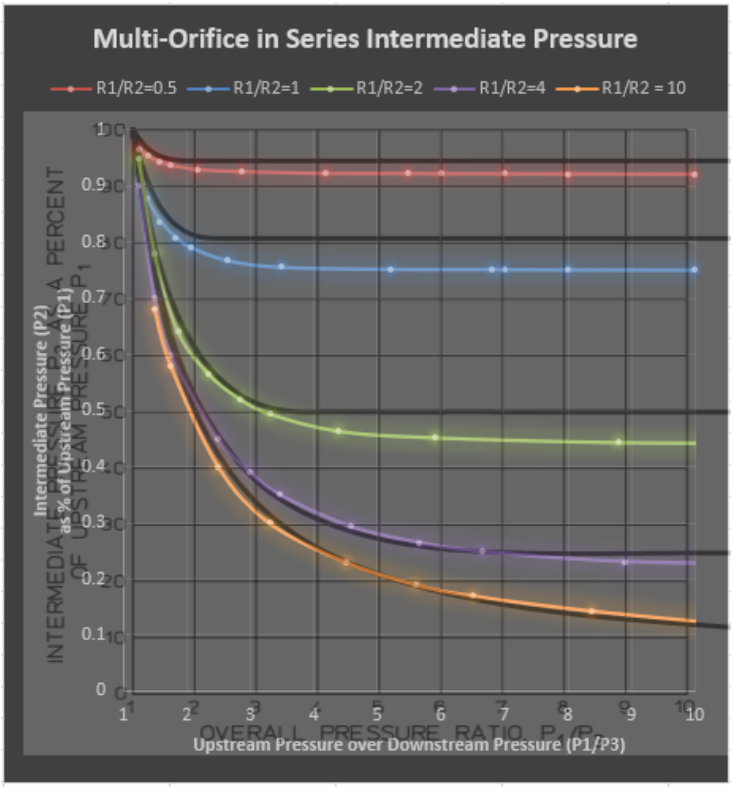

Figure 54: Multi-Orifice Data Comparison to Lee [6]

Restriction Ratio	Constant P2 Percentage of P1 (LEE)	Constant P2 Percentage of P1 (CFD)	Difference
0.5	0.95	0.925	2.5%
1	0.8	0.75	5%
2	0.5	0.44	6%
4	0.25	0.228	2.2%
10	0.1	0.084	1.6%

Table 18: CFD vs Theoretical Intermediate Pressure as Percentage of Upstream Pressure

The amount that the curves are off are similar to the percentage error of the single orifice theoretical vs experimental values and the experimental to the CFD values.

4.0 DISCUSSION

4.1 Discussion of Results and Analysis

As discussed in the previous report [1], “solutions within the theoretical portions of this report should be considered only an approximation to the solution since many assumptions were made that neglect real world compressible flow. For a more exact solution, the experimental data shall be consulted”. Since experimental data was collected during the single orifice and validated with CFD, there can be more certainty using these programs if setup and optimized correctly as was conducted in this report. Though the numerical approach was very accurate in comparison to the experimental results, many assumptions were made, and experimental results will be most accurate data collection method. If time is of the essence, and many configurations need to be considered, then numerical approaches can be used.

Error between the experimental and theoretical approaches was discussed in the previous report [1] which relied heavily on the theoretical results where this report is targeted toward the numerical and experimental. When considering the numerical approach, many errors can occur which make the values deviate. The CFD does match closer to the experimental since it accounts for many of the real world factors that the theoretical calculations does not. Where the error comes into play is the optimization of the mesh. If not set up correctly, the values will be entirely off as seen in the mesh convergence study. Once the values converge, the error is much less and the mesh can be seen as optimized, where more refinement will not improve the calculations as much. One source of error noticed at the scale the models were made to is the coefficient of discharge. It is assumed to be a sharp edge, but with a 0.0007” hole in a 0.005 plate, the edge is not sharp. In fact, the

discharge coefficient is impacted by the length to diameter ratio (L/D). There are coefficient of discharge coefficients for such situations, but mainly when the L/D ratio is equal to unity. In this case, it is well over unity and many variations and shock waves can be observed in the orifice depending on the flows and pressures. It was seen in the single orifice validation, the upstream pressure was not exact, though the same flow rates were used. This could be due to small errors in the mesh, the discharge coefficient assumption, or even the density of the gas. The experimental data was collected in volumetric flow and to use in the numerical analysis, the volumetric flow needed to be converted to mass flow using the assumed density of the gas, which many not always be constant.

The pressure ratio impact shown in Table 17 shows great insight into the instances where an orifice would be sonic or subsonic. P1/P2, P2/P3, and P1/P3 were all evaluated. It is noted that when P1/P3 is subsonic, neither of the orifices become sonic since the velocities are not high enough to reach the critical speed of sound. This table can be used for customers that are concerned with efficiency in their propellant management systems where they need to ensure a constant mass flow. They will be able to see how the orifices will perform when an upstream and downstream pressure are specified in their system.

The solving of the intermediate pressures was especially informative in that solving for various restrictions in series, the plots were able to be developed to match what had been established from theoretical calculations [6]. With CFD, the pressure ratios were able to range higher as to give more insight into the consistency of the pressures when the P1/P3 pressure ratio was up to 25 when

the Lee Company chart stopped at 10. This didn't allow for clarity on the restriction ratio of 10, but with the parametric study, the picture is much clearer.

With the very close agreement between these graphics, at a maximum of 6% and an average of 3.46%, the numerical analysis can be used to produce similar graphics when setting more than two orifices in series. This will be advantageous for industries looking to produce high restriction orifices with larger hole sizes due to contamination. They will not have to produce micro-orifices just to high the restriction. They could use many larger holes instead of two miniature orifices and obtain the same results but have an understanding on the fluid behavior at each orifice.

When aiding in the design of propellant management systems, the orifices used can be either tested or theoretically calculated. Exact flow requirements may have to be experimentally collected, but if time is of the essence, this data shows that with proper mesh optimization and proper setup, numerical approaches can be used with results that are close enough in agreement with both experimental and theoretical calculations that the results can be confidently presented. Another advantage is the ability to perform multiple design cases using parametric studies. This is helpful when a customer has a complex system with many cases or is not confident in proposing just one requirement. The future work explained in the next section of this report will give even more insight into the use of multiple orifices in many configurations. This report acts as a valid steppingstone for more advanced work and will continue after this report concludes.

4.2 Future Work

Due to time constraints, studying the impact of a longer series of orifices was not conducted. The impact of the intermediate pressure when for example three or four orifices are in series would be interesting. This would yield more useful information for high restriction components with larger passage sizes (many more orifices in series). There have been components that have up to 120 orifices in series for both incompressible and compressible fluids, but with the non-uniform pressure drop seen with compressible fluids across multiple orifices, it is hard to predict the intermediate pressures and resulting pressure ratios at various points in the series. An equation that could predict the intermediate pressures and sonic/subsonic conditions within the series based on the number of orifices would lend itself well to the design of thruster components.

For correlation purposes, other gases can be explored on the multiple orifices in series. This will allow an understanding of the performance of the gases of differing densities and purities. Some gases such as Helium are in short supply, so it would be advantageous to obtain data. Helium is also used as a correlating gas to many of the inert gases used in the propulsion systems such as Krypton and Xenon.

At least on a small scale, it would be advantageous to test these multiple orifices in series experimentally to verify the curves. With the data collected for the single orifice compared to the theoretical and numerical approaches, it seems that they should all match well, but for further support of the multi-orifices in series.

Lastly this method of numerical study should be used to investigate the impact of orifices in a parallel circuit as this type of setup can be commonly used in many manifold type setups for space industry propulsion. Even more complex is the fact that many highly restrictive multi-orifice series restrictors are placed in a parallel setup. Since numerical analysis uses less resources and time, it should be taken advantage of.

REFERENCES

1. Navin, Ian. “Pressure Ratio Impact on Compressible Fluid Flow Through a Laser Drilled Single Orifice Restrictor (Theoretical and Actual Edge Conditions).” Rensselaer Polytechnic University, 2022.
2. Zucrow, Maurice Joseph, and Joe D. Hoffman. Gas Dynamics. Wiley, 1976.
3. Sadegh, Ali M., and William M. Worek. Marks' Standard Handbook for Mechanical Engineers. McGraw-Hill Education, 2018.
4. https://www.theleeco.com/insights/selecting-accurate-flow-control-restrictors-for-electric-propulsion/
5. http://67.199.46.28/engineering/gases/gas-flow-characteristics.cfm
6. https://www.ddp.nl/wp-content/uploads/2020/07/Precision-Hydraulics-12th-Edition-2019.pdf
7. https://www.okeefecontrols.com/wp-content/uploads/Choked-Flow-of-Gases-pg-48.pdf
8. https://www.aft.com/documents/AFT-Modeling-Choked-Flow-Through-Orifice.pdf
9. https://www.nrc.gov/docs/ML1214/ML12142A162.pdf
10. http://willson.cm.utexas.edu/Teaching/Che253M/Files/EXP%202%20Compressible%20Gas%20Flow%2008-15.pdf
11. Goebel, Dan M, and Ira Katz. Fundamentals of Electric Propulsion : Ion and Hall Thrusters. Wiley, 2008. INSERT-MISSING-DATABASE-NAME, INSERT-MISSING-URL. Accessed 23 May 2022.
12. https://ntrs.nasa.gov/api/citations/19850010711/downloads/19850010711.pdf
13. http://mae-nas.eng.usu.edu/MAE_6530_Web/New_Course/Section3/compressible_orifice.pdf
14. https://www.nasa.gov/centers/glenn/technology/Ion_Propulsion1.html

APPENDIX

Multi-Orifice Cut Plots (Front Plane)

- $\frac{R1}{R2} = 0.5$

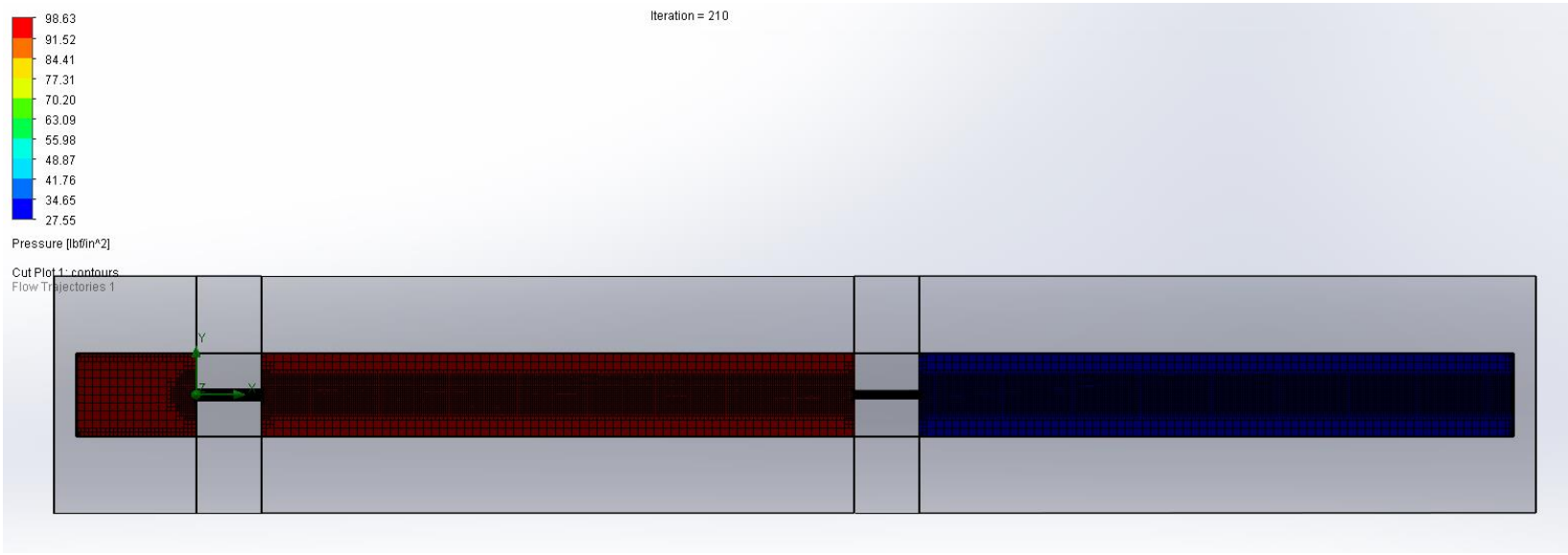

Figure 55: R1/R2=0.5 Pressure Cut Plot (Full View)

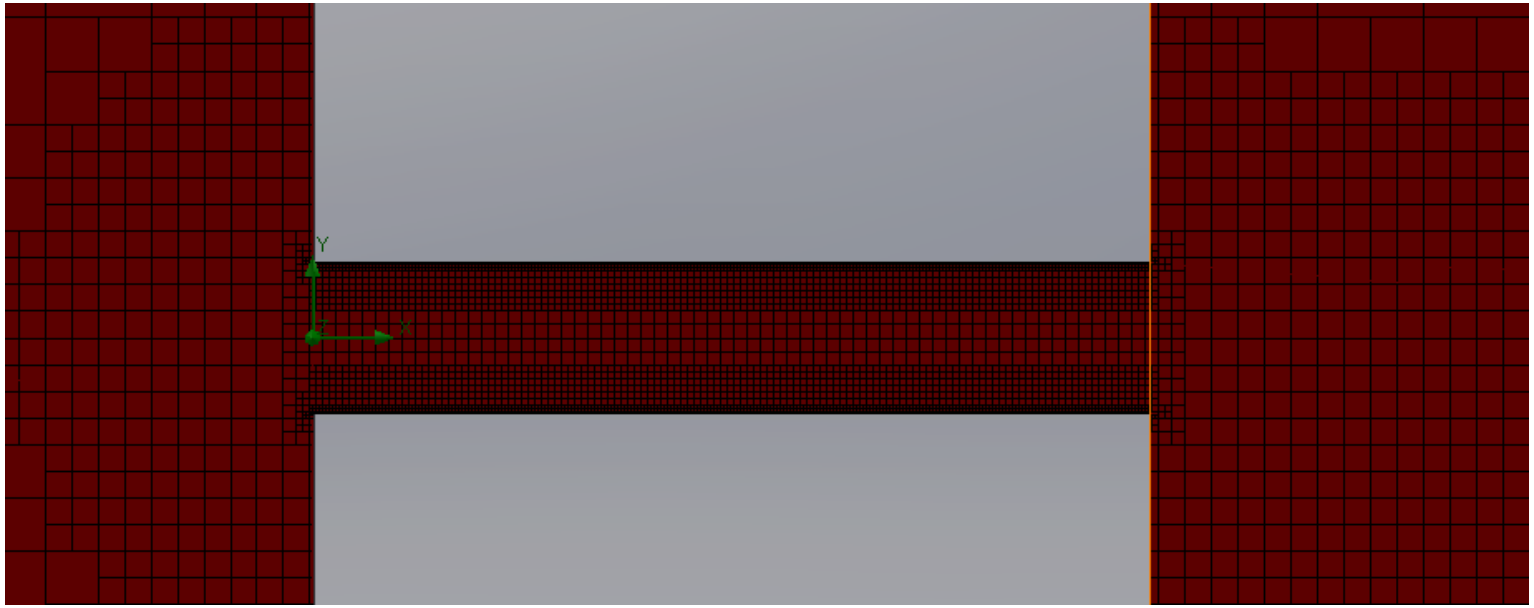

Figure 56: R1/R2=0.5 Pressure Cut Plot (Orifice 1)

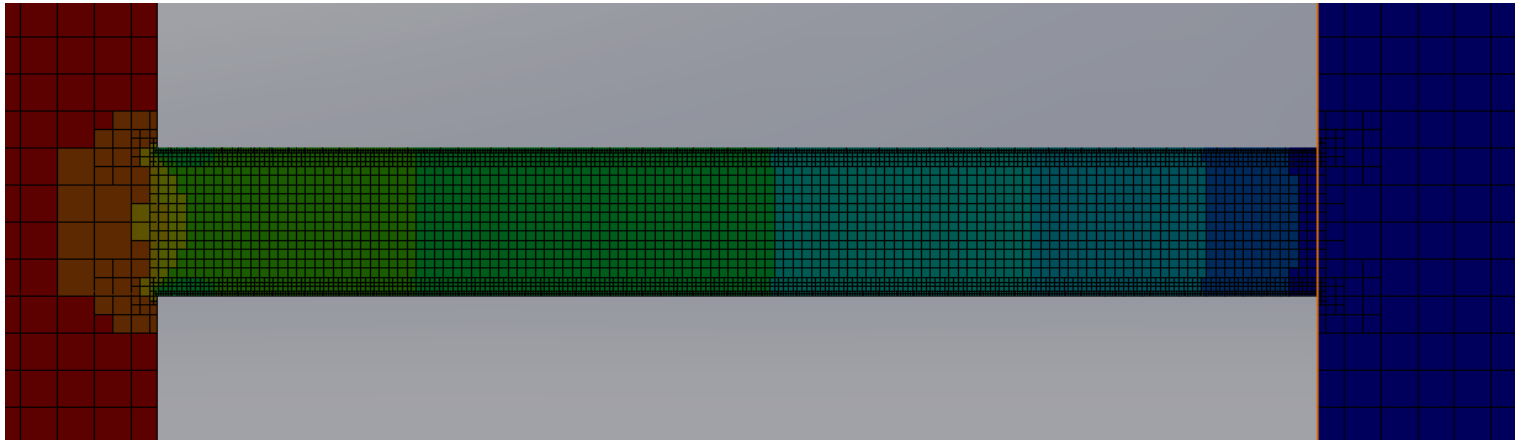

Figure 57: R1/R2=0.5 Pressure Cut Plot (Orifice 2)

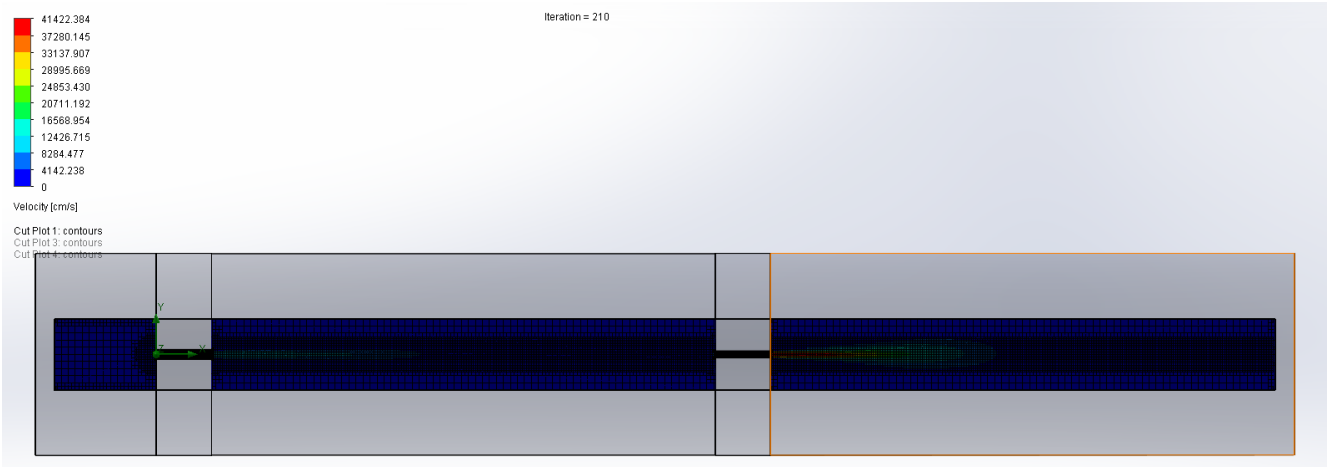

Figure 58: R1/R2=0.5 Velocity Cut Plot (Full View)

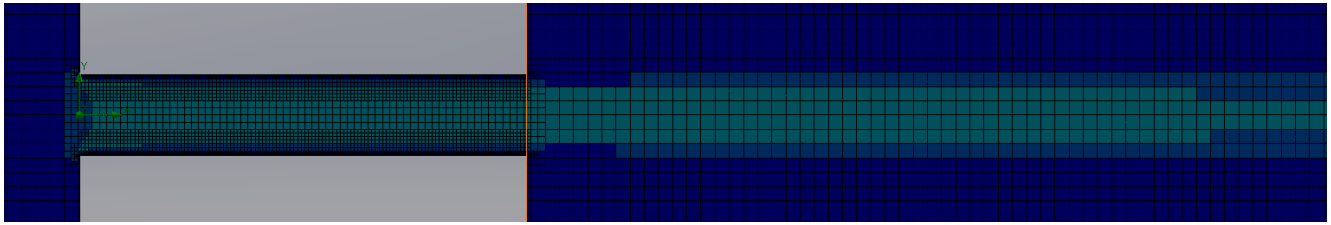

Figure 59: R1/R2=0.5 Velocity Cut Plot (Orifice 1)

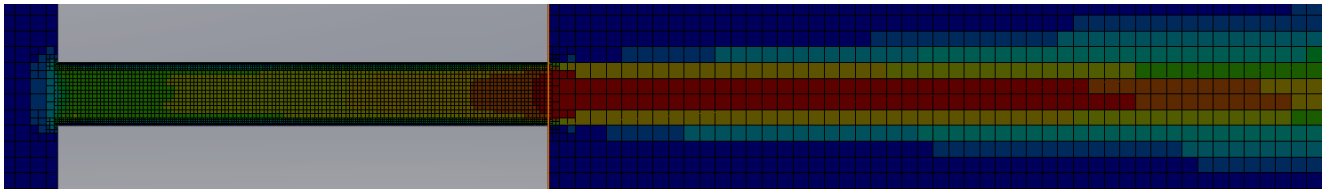

Figure 60: R1/R2=0.5 Velocity Cut Plot (Orifice 2 Zoom)

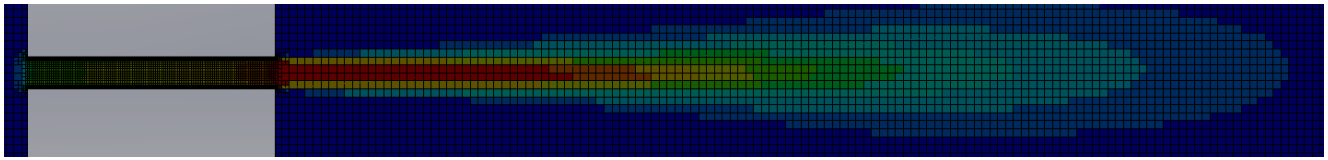

Figure 61: R1/R2=0.5 Velocity Cut Plot (Orifice 2)

- $\frac{R1}{R2} = 1$

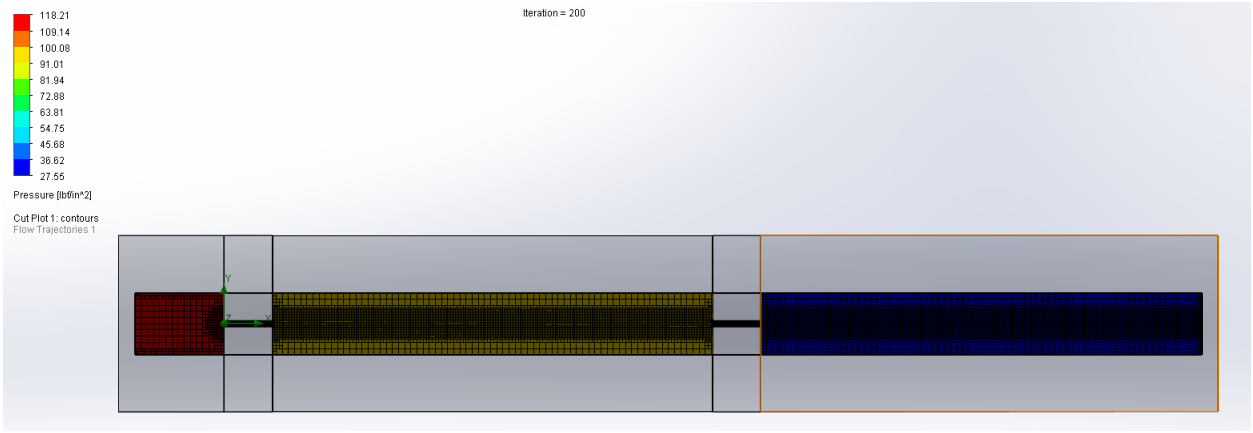

Figure 62: R1/R2 = 1 Pressure Cut Plot (Full View)

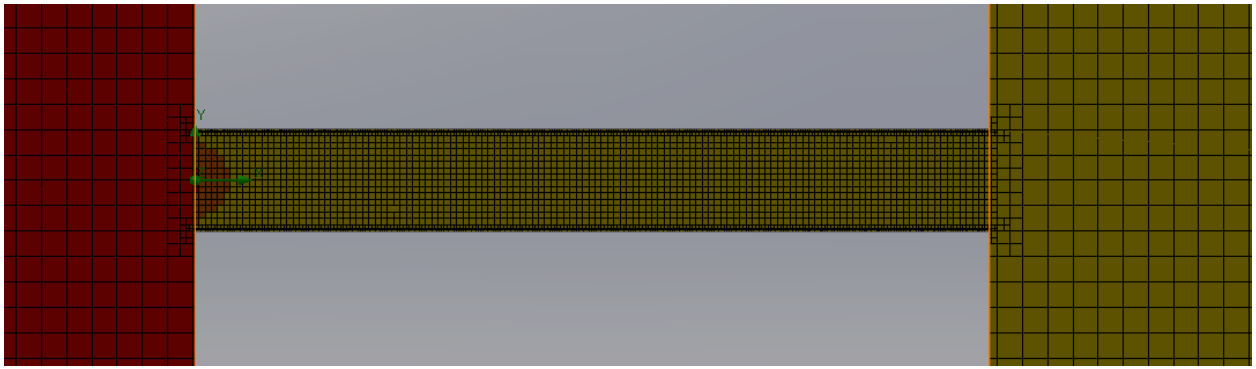

Figure 63: R1/R2 = 1 Pressure Cut Plot (Orifice 1)

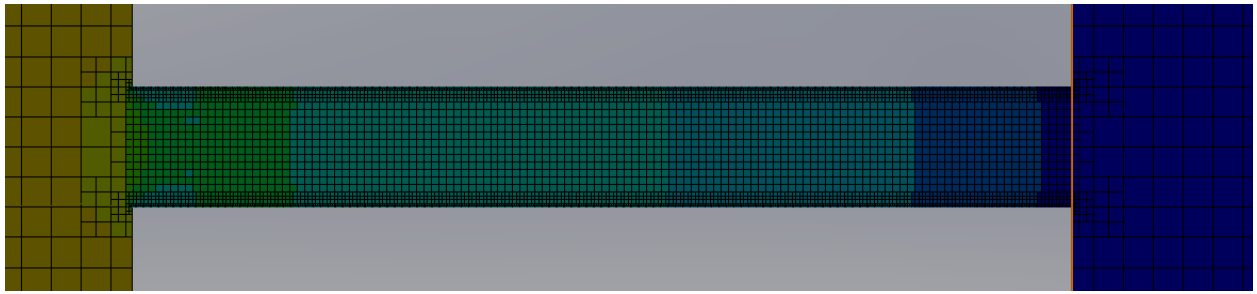

Figure 64: R1/R2 = 1 Pressure Cut Plot (Orifice 2)

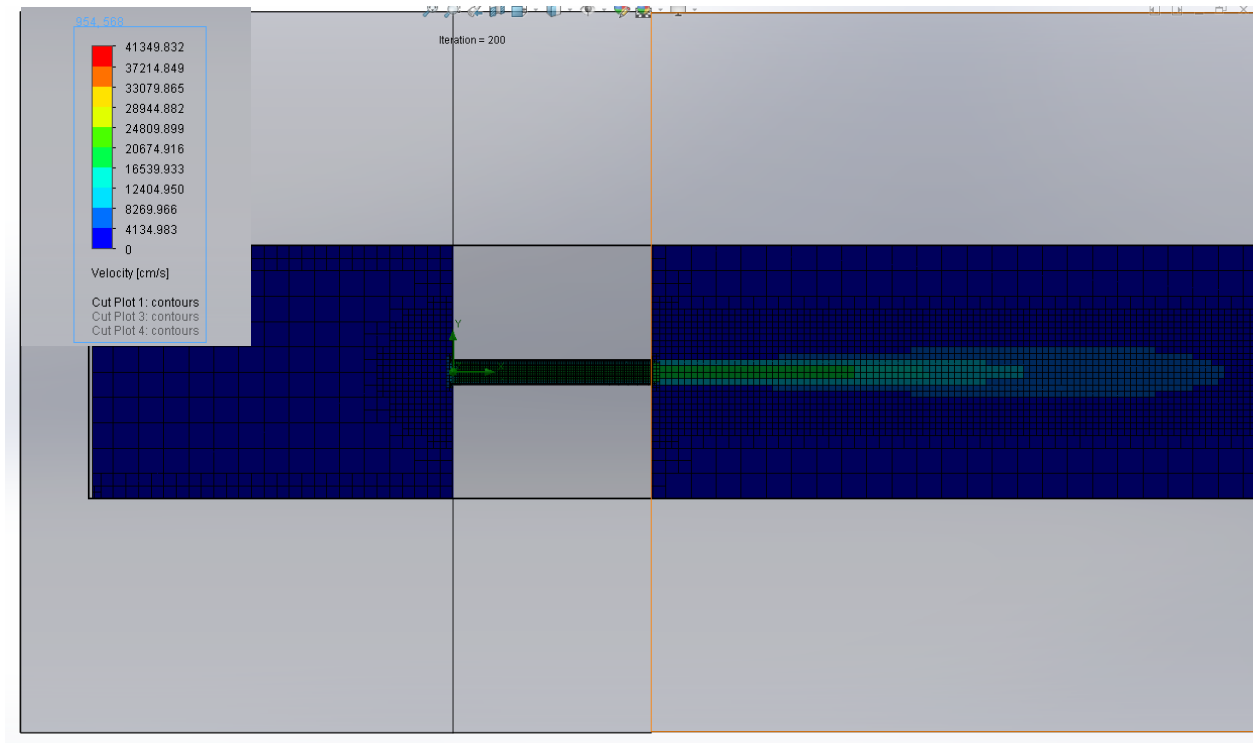

Figure 65: R1/R2 = 1 Velocity Cut Plot (Orifice 1)

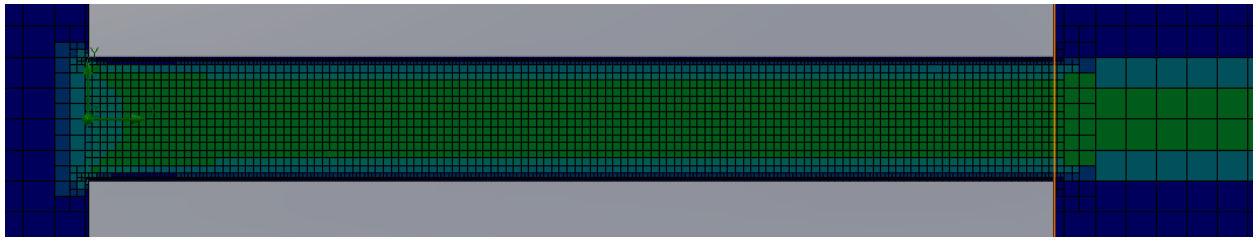

Figure 66: R1/R2 = 1 Velocity Cut Plot (Orifice 1 Zoomed)

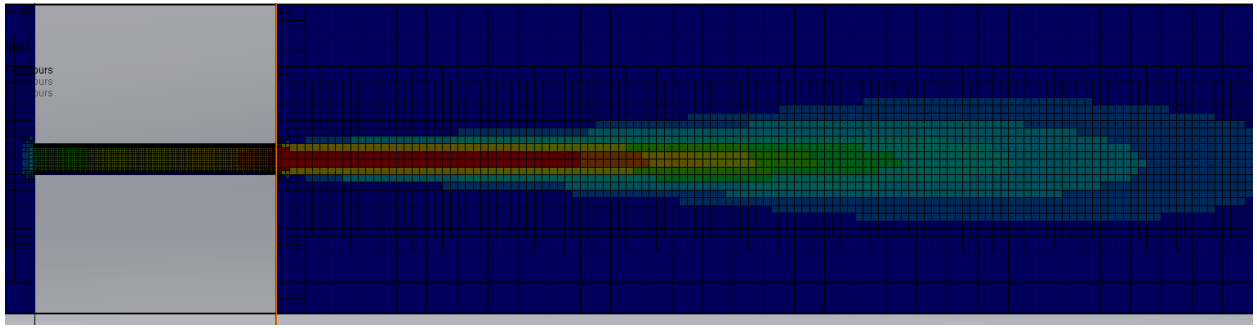

Figure 67: R1/R2 = 1 Velocity Cut Plot (Orifice 2)

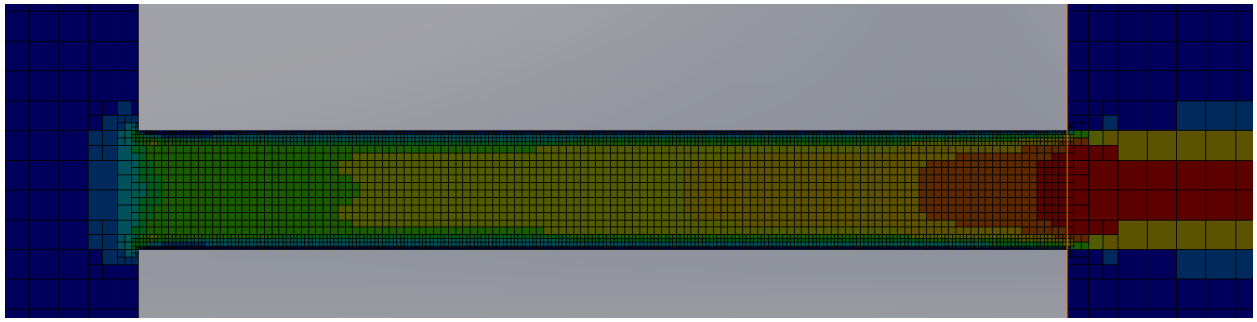

Figure 68: R1/R2 = 1 Velocity Cut Plot (Orifice 2 Zoomed)

- $\frac{R1}{R2} = 10$

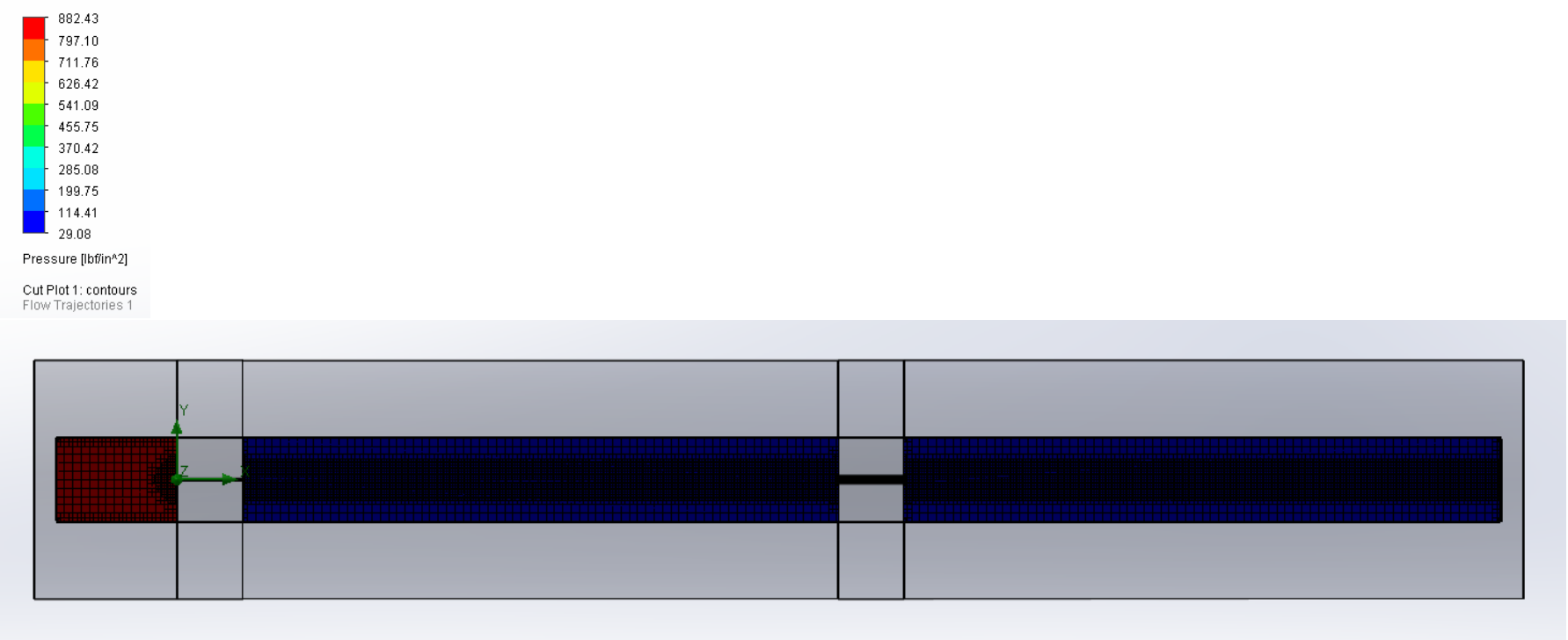

Figure 69: R1/R2 = 10 Pressure Cut Plot (Full View)

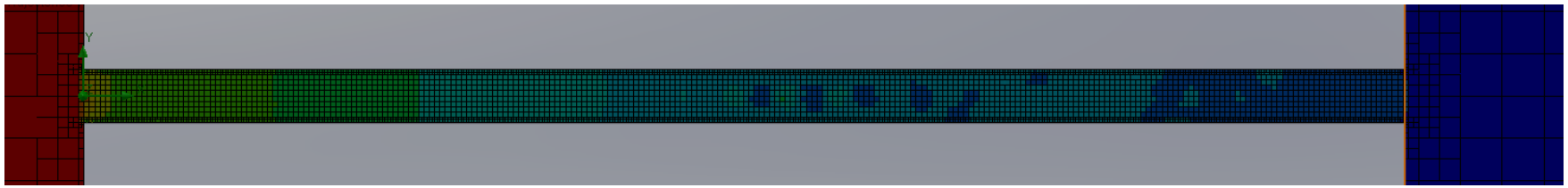

Figure 70: R1/R2 = 10 Pressure Cut Plot (Orifice 1)

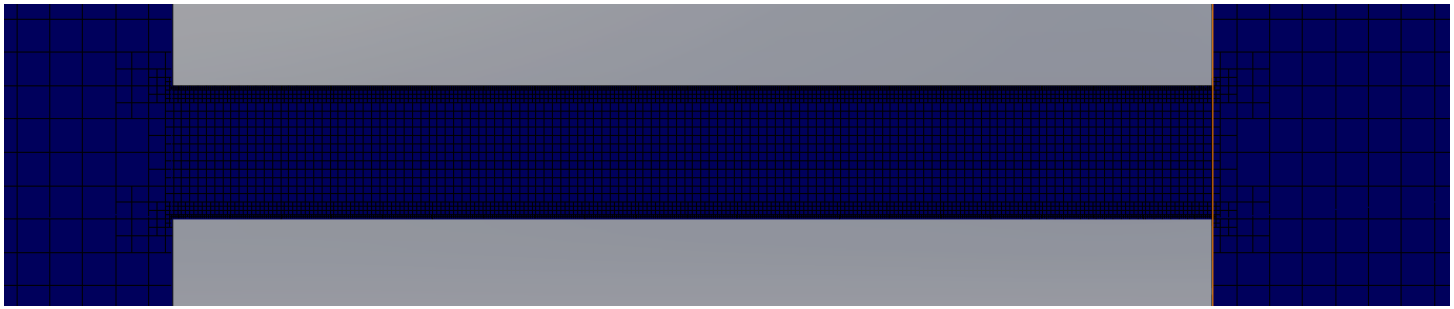

Figure 71: R1/R2 = 10 Pressure Cut Plot (Orifice 2)

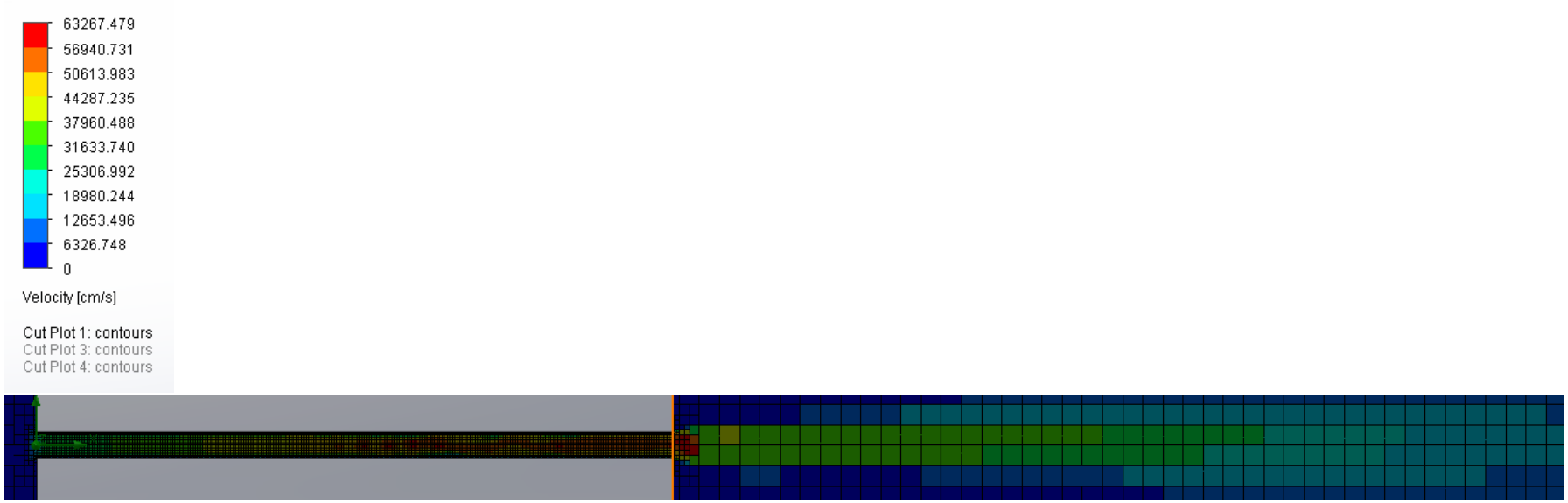

Figure 72: R1/R2 = 10 Velocity Cut Plot (Orifice 1)

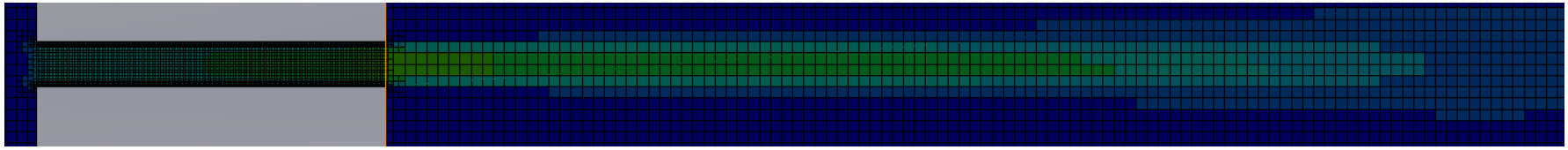

Figure 73: R1/R2 = 10 Velocity Cut Plot (Orifice 2)